Arabian Journal for Science and Engineering
https://doi.org/10.1007/s13369-023-08426-z

RESEARCH ARTICLE-CIVIL ENGINEERING

Long-Term Response of Piled-Raft Foundations Subjected to Incremental Compressive Loads

Kajal Tarenia[1] · Nihar Ranjan Patra[1] · Sathiyamoorthy Rajesh[1] · Apurba Mondal[2]

Received: 14 December 2022 / Accepted: 19 October 2023

Abstract
In this manuscript, the long-term behaviour of piled-raft foundations (PRFs) due to the consolidation of clayey soils has been investigated by 3D finite element analysis. The validation of the numerical prototype has been carried out using the field test outcomes performed in the field laboratory and other reported results. The ultimate load capacity of the PRFs has been assessed by varying the number of piles, diameter of piles, width of raft and ground water level. Compressive loads are provided starting from an increment of 10% of the ultimate load till the ultimate load capacity of the PRFs. Settlements of PRFs have been observed till a time period of 1 month for each increment of loading and for a period of 1 year after the ultimate load capacity has been applied. The influence of load sharing behaviour, interaction effects and factor of safety on consolidation settlement of PRFs have been analysed, and predicted expressions are suggested. Average, differential and reference settlements are evaluated. Multiple linear regression analysis is implemented for estimating consolidation settlement. The proposed design equation has been validated using an example. It is inferred that load sharing ratio increased by about 34–48%, 6–19% and 11–20% with increase in the number of piles, pile diameter and width of raft in the PRF, respectively. The reduction rate of factor of safety of PRFs is insignificant and nearly minimizes to a constant value at higher settlement magnitude. The reference settlement increases from 49 to 54% as the value of load sharing ratio decreases.

Keywords Piled-raft foundation · Consolidation settlement · Time effect · Load sharing ratio · Interaction factor · Factor of safety

1 Introduction

The soar in the shortage of land and requirement of multistorey buildings, offshore structures, bridges and towers have remarkably extended the usage of piled-raft foundations (PRFs) [1]. The entire performance of the structure is improved, and the total and differential settlements are controlled by the use of PRFs [2]. Piles carry out the role of settlement reducer, while the raft provides stiffness and soil resistance in a PRF [3]. PRFs are being used for tall buildings and structures based on several field studies reported earlier [4–6]. The combined action of PRF produces overlapped stresses and strains below the foundation because of the interaction among various foundation components. The interactions lead to variations in the load-carrying capacity and settlement resulting in different proportions of load-carrying capacities of individual foundation components [7]. The long-term behaviour (time effect) of PRFs in clayey soils is crucial as the stresses and strains continue to change after the construction of the superstructure is completed.

Several experimental and numerical studies have been reported on PRFs monitoring the load–settlement response, load sharing response and bending moment behaviour [8–12]. Cho et al. [8] investigated the load–settlement response of a square PRF in clayey soil using ABAQUS

✉ Nihar Ranjan Patra
nrpatra@iitk.ac.in

Kajal Tarenia
kajal@iitk.ac.in

Sathiyamoorthy Rajesh
hsrajesh@iitk.ac.in

Apurba Mondal
apurba@npcil.co.in

[1] Department of Civil Engineering, Indian Institute of Technology, FB-316, Faculty Building, Kanpur, Uttar Pradesh 208016, India

[2] Nuclear Power Corporation of India Ltd., New Delhi, India

Published online: 08 December 2023

software. Their main focus was to quantify the minimization of differential and average settlements in stiff and soft clayey soils. They reported that the differential settlement was decreased by providing piles in the central area of the raft and the average settlement was reduced by using widely spaced pile groups. However, the consolidation effect was not considered for the PRFs. Chung Nguyen et al. [9] conducted centrifuge tests and parametric study using PLAXIS 3D Foundation on PRFs considering flexible rafts in homogeneous dry sand. They reported that PRF consisting of piles arranged in a concentrated manner could reduce the total and differential settlements than PRFs with uniformly arranged piles. Deb and Pal [10] analysed the load sharing and interaction factors of PRFs subjected to vertical loads. Halder and Manna [11] evaluated the interaction factors of PRFs in sand subjected to vertical load by the use of a centrifuge and found that the curve between interaction factors and the settlement were nonlinear in nature. Mali and Singh [12] conducted parametric study considering the effect of length, spacing and diameter of piles, raft–soil stiffness ratio, load sharing, shear force and bending moment on the behaviour of large PRF. They reported that the load sharing ratio was reduced as the spacing of piles was increased, whereas the load sharing ratio was increased as the length of piles was increased. However, the reported studies considered only the immediate settlement of the foundation. Also, the effect of water table and consolidation was not considered in their studies. It is clear from the preceding studies that large-scale tests (field tests) on PRFs remain largely unexplored and the consolidation settlement with respect to time has been neglected in case of PRFs. The excess pore water pressure variation and the settlement calculation due to the change in water table also have not been performed in the previous studies.

A limited amount of research has been reported on PRFs considering the consolidation settlement of soils with respect to time [13–21]. Rodriguez Rincon et al. [15] performed tests in a centrifuge considering different orientation of piles beneath the raft and investigated the effect of consolidation and water extraction from the soil layer on the behaviour of PRFs. They reported that the water extraction from the soil layers deep below gave rise to greater settlement. Tarenia and Patra [18] conducted numerical analyses on disconnected and connected PRFs subjected to varying horizontal loads maintaining constant compressive load over a period of 20 years. They concluded that excess pore water pressures in disconnected piled-raft foundations were 50–63% higher than in connected piled-raft foundations. However, the discussion on load sharing ratio and interaction factors with respect to the consolidation settlement of PRFs had not been reported. Thaher and Jessberger [20] conducted centrifuge tests in clay soil and analysed the variation in the number, length and diameter of piles on the settlement response. They also analysed the load sharing of each element (raft and pile) in various models of PRFs. However, they did not consider the influence of pore water pressure and change in the groundwater level.

The load transfer mechanism of PRFs is complicated because of the joint effort of piles and raft. An ample amount of the literature has been reported where the load sharing mechanism has been idealized in terms of geometry and stiffness of the foundation as well as soil compressibility [7, 22–24]. Lee et al. [7] conducted centrifuge tests on PRFs and reported that the load sharing ratio decreased as the settlement increased depending on the load capacity. However, it is crucial to investigate the load sharing mechanism and load–settlement behaviour by calculating the load sharing ratio (LSR) and load distribution coefficient (LDC) for an efficient PRF design. Furthermore, the relationship between the load sharing ratio and interaction factor has not been recognized. Also, PRF design relating factor of safety with the consolidation settlement is unexplored. The interaction effects of PRFs can be classified as pile–pile, raft–pile and pile–raft interactions [5]. The load-carrying capacity of group piles is less than for piles in PRFs due to raft–pile interaction effects [25]. According to Han and Ye [26], settlements caused due to the loading on the surface of raft lead to reduction in pile shaft friction owing to the reduction in settlement between the piles and neighbouring soils. Extensive experimental and analytical investigations have been reported earlier on the interaction effects of PRFs [27–29]. Conte et al. [30] performed centrifuge tests on PRFs and concluded that the raft in PRFs contributed to the additional foundation stiffness. Park and Lee [31] inspected the interaction effects of PRFs embedded in sand. From the above discussion, it may be concluded that most of the studies are based on the load capacity and interaction effect of piles and raft considering that the load-carrying capacity is fully mobilized at the ultimate condition. Research on the variation of interaction effect with time-dependent settlement is largely unexplored so far.

Based on the previous studies, it is revealed that the long-term response of PRFs, i.e. the influence of consolidation settlement with time considering variation in the number and diameter of piles, width of raft and ground water level, remains largely undiscovered. The excess pore water pressure variation with respect to time considering the above parameters has not been reported so far. Also, the load sharing behaviour, interaction effects and factor of safety of PRFs subjected to incremental compressive loading with time effect (considering the consolidation settlement) have not been explored. It is evident from the previous studies that validation of the numerical models with field tests on PRFs subjected to compressive loads taking into account time effects is very scarce. In this context, first the ultimate load capacity (ULC) of the PRFs has been assessed by variation in the number and diameter of piles, width of raft and ground water level. In the second analysis, compressive loads

have been provided starting from an increment of 10% till the ultimate load capacity of the PRFs. The settlement corresponding to each increment of loading has been observed till a period of 1 month, and the final (consolidation) settlement corresponding to the ultimate load capacity has been observed till a period of 1 year. The variation in the excess pore pressure with respect to time has been calculated for various configurations of PRFs. The analyses have been carried out by the 3D finite element software PLAXIS 3D [32]. The numerical model has been validated using the field load test outcomes performed in the field-testing laboratory of the Indian Institute of Technology Kanpur (IITK) and the numerical results reported by Cho et al. [8]. The properties of the sub-soil for the numerical analysis are taken as per the soil profile of IITK considered in the field study. Based on the numerical analyses conducted on PRFs considering the above parameters (number and diameter of piles, width of raft and ground water level), equations have been developed to predict the LSR, interaction factors and factor of safety (FS) with reference to the final (consolidation) settlement of PRFs. The average, differential and reference settlements of PRFs with respect to time have been analysed. In this study, a new method for the evaluation of interaction factors and load sharing ratio of PRFs has been suggested considering time effects. A regression analysis has been implemented for estimating consolidation settlement and for achieving a suitable design of PRF in Kanpur soil by the use of simplified expressions.

2 Numerical Modelling of the PRF

A three-dimensional FE analysis of a PRF subjected to axial compressive loading considering time effects has been carried out by PLAXIS 3D software. The raft is located above the ground surface, and the piles are placed below the ground surface rigidly connected to the raft. The diagrammatic illustration of the piled-raft foundation (PRF) is shown in Fig. 1. Figure 1 shows the load applied to the PRF (Q) exhibiting different interactions such as pile–raft interaction (P–R), raft–pile interaction (R–P) and pile–pile interaction (P–P). The skin resistance of piles and the end-bearing capacity (Q_b) of the piles are also shown. The soil deposit is layered consisting of 13 layers, and the soil properties are obtained from the soil tests performed on the soil of the IITK field laboratory. The structural elements, that is, piles and raft, are considered to be made of concrete. Figure 2 shows the characterization of the PRF indicating the point of application of load, discretization of the finite element mesh and its dimensions. Mesh optimization is performed to determine the boundary extent which assisted in minimizing the computational attempt. The horizontal extremities of soil are taken

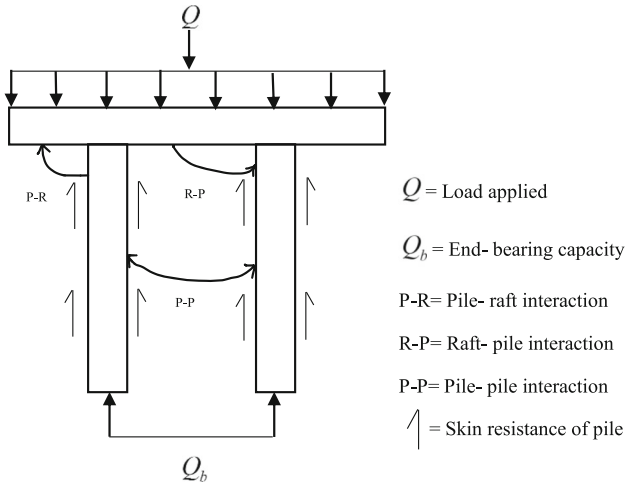

Fig. 1 Diagrammatic illustration of the piled-raft foundation (PRF)

equal to 15 times the raft width ($15B_r$). The vertical extremity is adopted to be 2.5 times the length of the pile ($2.5L$) to minimize the boundary effects. The horizontal motion of the side edges of the soil bed remains constrained. The bottommost surface of soil bed has been held fixed in vertical and lateral directions. The lateral boundaries and the bottom boundary of the soil are kept open (i.e. fully drained boundary condition has been adopted allowing excess pore water pressure to dissipate freely). The top boundary (Z axis) is kept open in the analysis as there should be free flow (zero excess pore pressure) across the surface, which resembles the actual field condition. The soil model consists of 10-noded tetrahedral soil elements. The soil bed has been meshed by variation of mesh density. A coarseness factor of 0.25 is provided to the mesh. Local mesh refinements have been allocated close to the PRF where accumulation of deformation gradient as well as stress is expected to be higher. The fine mesh is nearest to the PRF. This has been done for establishing efficiency and accuracy in the numerical analysis. The hardening soil (HS) model has been considered for the soil as suggested elsewhere [33, 34]. The soil is considered as a nonlinear elastic perfectly plastic material. A basic characteristic of the hardening soil model is that the soil stiffness depends on stress. It has been established on the hyperbolic interrelation linking deviatoric stress and axial strain. It also favours the stiffness dependency with confining pressure, given as:

$$E_{50} = E_{50}^{\text{ref}} \left(\frac{c \cos\phi - \sigma_3 \sin\phi}{c \cos\phi + p^{\text{ref}} \sin\phi} \right)^m \tag{1}$$

where E_{50}^{ref} is the reference stiffness modulus with respect to the reference confining pressure $\left(p^{\text{ref}}\right)$; σ_3 is the minor principal stress; c is the cohesion; and ϕ is the friction angle. The actual stiffness depends on σ_3. The quantity of stress dependence is provided by the power law (m). The power

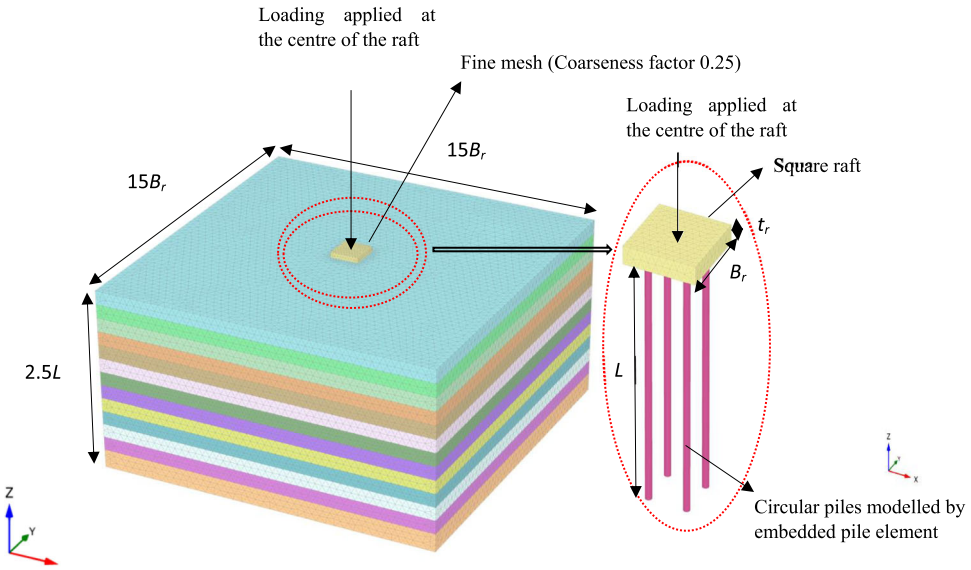

Fig. 2 Characterization of the PRF indicating the point of application of load, discretization of the finite element mesh and its dimensions

(m) is taken as 1 in case of soft clay [35] to replicate logarithmic compression behaviour. m is taken as 0.5 in the case of sandy soil [36]. Additional details regarding HS model can be obtained from the material model included in the PLAXIS 3D manual [37]. The value of Poisson's ratio is taken as 0.35, and the value of the strength reduction factor (R_{inter}) is taken as 0.5 for low plasticity clay to intermediate plasticity clay as recommended elsewhere [37]. The detailed sub-soil profile is given in Table 1. The properties of the 13 soil layers considered for the finite element modelling are given in Table 2. Sub-soil exploration has been conducted in the site up to a depth of 20 m. Disturbed and undisturbed soil samples have been collected, and laboratory tests have been conducted for soil classification purposes. Standard penetration tests (SPT) using a standard split spoon sampler have been performed at an interval of 1.5 m till 20 m depth. Properties of 13 soil layers have been obtained at an interval of 1.5 m till a depth of 20 m. The water table has been obtained at 7.5 m depth. It has been observed from the soil classification that Kanpur soil consists of low plasticity clay to intermediate plasticity clay with clay percentage varying between 6 and 22%. The typical grain size distribution curve for soils at depths of 3 m, 6 m, 9 m and 13.5 m is shown in Fig. 3a. The permeability tests have been performed to find the coefficient of permeability of soil samples till a depth of 20 m at an interval of 1.5 m. The coefficient of permeability ranges from 8.60×10^{-10} to 3.5×10^{-9} m/s. Pressuremeter tests have been carried out till a depth of 20 m at an interval of 1.5 m. The values of coefficient of earth pressure at rest are obtained from the pressuremeter test. The typical pressuremeter deformation curve of applied pressure versus volume at a depth of 13.5 m is shown in Fig. 3b. The creep volume versus corrected pressure at a depth of 13.5 m is shown in Fig. 3c. The applied pressure versus volume curves includes the pipe calibration, air calibration, field curve and corrected curve. The deformation curve in Fig. 3b has three phases, namely (i) the re-establishing phase (from origin to A), (ii) the pseudo-elastic phase (from A to B) and (iii) the plastic phase (from B to C). The walls of the borehole get relaxed after the augers are removed from the borehole. The cavity volume is hence reduced. Initially, when the probe is inflated, the borehole walls are forced back to their initial position. Point A indicates where the volume of the hole is returned to its initial phase. The straight-line portion of the curve between A and B is called the pseudo-elastic phase. It resembles a straight line because of the elastic property of soil. Point B indicates that the creep pressure is achieved. At point B, the plastic phase starts and ends at Point C. Point C is asymptotic to the limit pressure, and at this point, the pressure stays constant in spite of increasing the volume. From Fig. 3c, it is observed that the in situ horizontal stress is 2 kg/cm^2 (2 bars) and the limit pressure is 18.1 kg/cm^2. The coefficient of earth pressure at rest at 13.5 m is hence obtained as 0.85 (Coefficient of earth pressure at rest = in situ horizontal stress/overburden pressure). The Poisson's ratio is taken as 0.35 (for silty clays of low and intermediate plasticity as stated by [4]). The hardening soil parameters and shear strength parameters have been found out by performing triaxial tests in the laboratory on the soil specimens gathered from the field site (IITK). The secant modulus (E_{50}) is obtained from the slope of a line drawn from the origin of the deviatoric stress versus axial strain diagram which intersects the curve at the point of interest. Figure 3d shows the method for obtaining E_{50} from the stress–strain diagram. Once E_{50} is obtained, the reference secant stiffness (E_{50}^{ref}) has been obtained from Eq. (1). The reference tangent stiffness ($E_{\text{oed}}^{\text{ref}}$) is a drained modulus and has been taken

Table 1 Detailed sub-soil profile

Depth (m)	SPT (*N* value)	Group symbol	Specific gravity	Liquid limit (%)	Plastic limit (%)	Plasticity index (%)	Gravel (%)	Sand (%)	Silt (%)	Clay (%)	Coeff. of uniformity (C_u)	Coeff. of curvature (C_c)	Compression index	Void ratio	Coefficient of permeability (m/s)
1.5	25	CL	2.65	30.4	20.3	10	11.6	5.8	71.8	11	33.3	8.33	0.135	1.4	1.15×10^{-9}
3	19	CI	2.65	41	25.6	15.3	0.04	3.8	74	22	NA	NA	0.17	1.25	8.60×10^{-10}
4.5	27	CI	2.65	38.8	23.4	15.4	0.3	6.6	75.3	18	NA	NA	0.162	1.28	9.85×10^{-10}
6	21	CL	2.67	27.3	17.2	10.1	2.1	6.4	85.2	6.4	13.3	3.33	0.12	1.33	3.20×10^{-9}
7.5	29	CL	2.66	32.4	22.2	10.2	0.3	7.0	80.7	12	30	7.5	0.153	1.37	2.11×10^{-9}
9	32	CL	2.68	28.4	18.3	10.1	0.7	3.9	88.6	6.8	11.5	2.88	0.128	1.32	3.5×10^{-9}
10.5	35	CI	2.67	35	22.9	12.1	0	2.2	83	15	14.6	1.93	0.156	1.30	1.05×10^{-9}
12	33	CL	2.65	31.7	22	9.68	11.8	10.3	66.1	12	22.2	0.88	0.15	1.35	1.12×10^{-9}
13.5	32	CL	2.65	29.3	20	9.22	1.9	6	81.8	10	20	4.05	0.13	1.36	2.12×10^{-9}
15	34	CL	2.69	29	20.9	8.1	5.1	5.2	79.4	10	20	6.05	0.13	1.35	2.13×10^{-9}
16.5	33	CI	2.65	38.3	23.3	15	1.4	6.4	74.7	17	NA	NA	0.161	1.26	9.80×10^{-10}
18	31	CL	2.69	27.2	17.1	10	2.2	8.2	83.2	6.3	16	4	0.12	1.29	3.30×10^{-9}
20	30	CI	2.65	38	23	14.9	0.3	10.4	72.1	17	NA	NA	0.16	1.23	9.82×10^{-10}

Table 2 Properties of the 13 soil layers considered for the finite element modelling

Soil layers	Depth (m)	Material model	Unsaturated unit weight, Y_{unsat} (kN/m^3)	Saturated unit weight, Y_{sat} (kN/m^3)	Reference Secant stiffness, E_{50}^{ref}(kN/m^2)	Reference Tangent stiffness, E_{oed}^{ref}(kN/m^2)	Unloading/reloading stiffness, E_{ur}^{ref}(kN/m^2)	Power for stress level dependency of stiffness (m)	Cohesion, c (kN/m^2)	Friction angle, ϕ(Degrees)	Dilation angle (Degrees)	Poisson's ratio	Interface reduction factor (R_{inter})	Lateral earth pressure (K_o)
1	1.5	HS	16.3	16.3	12,816	12,816	38,448	1	62.76	28	0	0.35	0.5	0.64
2	3	HS	15.65	15.65	12,290	12,290	36,870	1	82.35	25.6	0	0.35	0.5	0.80
3	4.5	HS	15.7	15.7	13,004	13,004	39,012	1	73.54	28.01	0	0.35	0.5	0.85
4	6	HS	16.8	16.8	12,221	12,221	36,663	1	39.22	33.2	0	0.35	0.5	1.31
5	7.5	HS	16.8	17.2	15,973	15,973	47,919	1	66.68	28.2	0	0.35	0.5	1.16
6	9	HS	17	17.6	14,255	14,255	42,765	1	41.18	33.3	0	0.35	0.5	1.12
7	10.5	HS	17.2	17.5	13,130	13,130	39,390	1	68.64	28.5	0	0.35	0.5	0.91
8	12	HS	16.8	17.1	18,781	18,781	56,343	1	63.74	29.8	0	0.35	0.5	0.86
9	13.5	HS	17	17.3	18,111	18,111	54,333	1	62.76	29.54	0	0.35	0.5	0.85
10	15	HS	18	18.1	14,228	14,228	42,684	1	62.76	31	0	0.35	0.5	0.94
11	16.5	HS	18	18.2	12,182	12,182	36,546	1	70.6	28.8	0	0.35	0.5	0.91
12	18	HS	18	18.2	17,407	17,407	52,221	1	39.22	34.6	0	0.35	0.5	1.10
13	20	HS	17.5	17.8	18,586	18,586	55,758	1	69.62	30.28	0	0.35	0.5	0.92

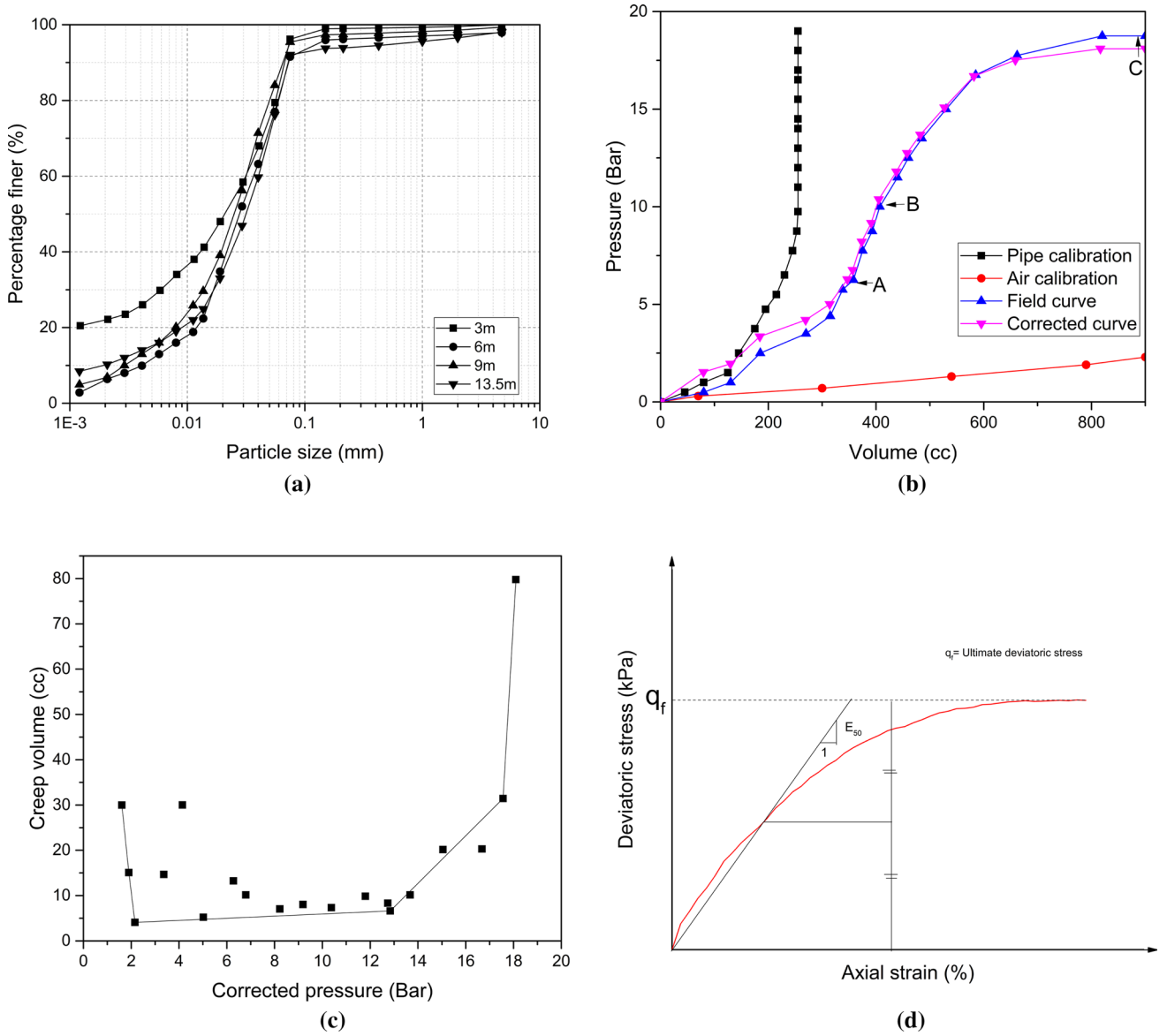

Fig. 3 **a** Typical grain size distribution curve for soils at depths of 3 m, 6 m, 9 m and 13.5 m. **b** Typical pressuremeter deformation curve of applied pressure versus volume at a depth of 13.5 m. **c** Creep volume versus corrected pressure at a depth of 13.5 m. **d** Method for obtaining E_{50} from the stress–strain diagram

equal to E_{50}^{ref}, and the unloading/reloading stiffness ($E_{ur}{}^{\text{ref}}$) has been taken equal to three times of E_{50}^{ref} [37]. According to Obrzud [38], the dilation angle is taken as zero considering the soil as normally consolidated or lightly consolidated cohesive soil. The square raft has been modelled as a plate element. Piles are modelled with the option of embedded pile element inbuilt in PLAXIS 3D. The piles and the raft are linear elastic in nature.

3 Method of Analysis

The analysis procedure contains the following steps:

- Firstly, the ultimate load capacities of un-piled rafts (URs) and PRFs have been obtained by providing incremental compressive loads at the centre of the raft. The ultimate load capacity has been obtained by the double tangent technique [39]. Only plastic analysis has been performed here to calculate the settlement of the PRF.
- Secondly, analyses are performed considering time effects. Vertical loading at the centre of the raft has been applied in increments of 10% of the ultimate load capacity of the PRF in each step till the ultimate load is reached. For each increment of loading, the settlement has been observed for a period of 1 month but after the application of ultimate load, the settlement has been observed for a period of

Table 3 Rate of loadings applied to the PRF for the analysis

Load applied to the PRF (kN)	Time duration of the application of load (Month)
10% of the ultimate load capacity	0–1
20% of the ultimate load capacity	1–2
30% of the ultimate load capacity	2–3
40% of the ultimate load capacity	3–4
50% of the ultimate load capacity	4–5
60% of the ultimate load capacity	5–6
70% of the ultimate load capacity	6–7
80% of the ultimate load capacity	7–8
90% of the ultimate load capacity	8–9
100% of the ultimate load capacity	9–21

1 year. Consolidation analysis has been carried out and the excess pore pressures have been measured with respect to time. The steps involved in the analysis are as follows:

i Initially K_0 procedure has been performed simulating stress condition under initial geometry configuration inbuilt in PLAXIS 3D.
ii The piles and raft are activated in the next step.
iii A point load equivalent to 10% of the ultimate load capacity (ULC) of the PRF has been applied at the centre of the raft. Time period of loading has been provided as 1 month. Consolidation analysis has been carried out. The values of the coefficient of permeability are provided in Table 1.
iv All the increments of loading till the ultimate load capacity of the PRF are provided step by step, and consolidation analysis has been carried out for 1 month for each step of loading.
v After the ultimate load capacity has been applied, the consolidation analysis has been carried out for a period of 1 year. The rate of loadings applied to the PRF for the analysis is presented in Table 3.
vi The final (consolidation) settlement is observed at the node just present below the centre of the raft. The excess pore water pressure, load sharing ratio, interaction factor and the factor of safety are observed.

4 Parametric Cases

Parametric studies considering the influence of several parameters like the number and diameter of piles and width of raft along with the change in ground water level have been performed to investigate the final (consolidation) settlement and excess pore water pressure of the PRFs with time. The load sharing ratio, interaction factors, factor of safety, differential settlement, average settlement and reference settlement of PRFs have also been investigated with time. The number of piles in the PRF is taken as 1, 4 (2 × 2 pile group), 9 (3 × 3 pile group) and 16 (4 × 4 pile group). The diameter of piles is taken as 0.4 m and 1 m. The length of the piles is taken as 8 m. The piles are symmetrically placed and rigidly connected to the raft. Raft sizes of 14 m × 14 m and 16 m × 16 m have been considered. The thickness of raft has been taken as 0.6 m for all the cases. The spacing between the piles is taken as 4 times the diameter of pile for all the cases. The influence of the various parameters has also been analysed for the case of un-piled rafts. The water table has been considered at the top of the soil layer (0 m), 7.5 m and 10 m, respectively. No water table case has also been considered for all the cases of PRFs. The various cases adopted for the parametric study are shown in Table 4.

5 Validation of the Numerical Model

The validation of the numerical model has been conducted using the field load test results performed in the field-testing laboratory of Indian Institute of Technology Kanpur (IITK) and the numerical results reported by Cho et al. [8] for static vertical loading case.

5.1 Field Load Tests

The PRF comprising of bored cast-in situ concrete piles (2 × 2 pile group) having diameter 0.4 m has been used in the load test. Spacing between the piles is 4*d*. (*d* represents the diameter of pile.) The properties of piles and raft considered for the field study are summarized in Table 5. The length of anchor piles and main piles are 10 m and 8 m, respectively. For the boring, the screw auger boring method has been followed. Piles have been installed by positioning 12 mm reinforcement steel bars in the centre of the auger bore and filling the bore with M25 grade concrete. Concrete has been mixed by a mechanical mixer and is dropped by chute. To get rid of the air bubbles and voids, a needle vibrator is used to maintain an even distribution of concrete. The piles are cured for 28 days preceding the test. An average temperature of 33 °C was measured during pile curing. Slump value of the concrete is obtained as 105 mm ensuring that the degree of workability is high. Compressive strength of concrete is obtained as 16.16 MPa and 25.84 MPa after 7 days and 28 days curing period, respectively. Strain gauges and load cells are instrumented to calculate the variation in strain and transfer of load at the pile head and pile tip. Strain gauges are instrumented along the pile lengths of P2 and P5. Five electrical strain gauges are installed in each reinforcement. A total number of two bars placed diametrically opposite to

Table 4 Various cases adopted for the parametric study

Type of foundation	Size of raft (m × m)	Diameter of pile(m)	*S/d* ratio	Denotation of the foundation (PR number of piles size of raft diameter of pile)
Un-piled raft	14 m × 14 m	Nil	Nil	UR-14
	16 m × 16 m	Nil	Nil	UR-16
Raft + 1 pile	14 m × 14 m	0.4	Nil	PR-1-14-0.4
	16 m × 16 m	1	Nil	PR-1-16-0.4
				PR-1-14-1
				PR-1-16-1
Raft + 4 piles	14 m × 14 m	0.4	4	PR-4-14-0.4
(2 × 2 pile group)	16 m × 16 m	1	4	PR-4-16-0.4
				PR-4-14-1
				PR-4-16-1
Raft + 9 piles	14 m × 14 m	0.4	4	PR-9-14-0.4
(3 × 3 pile group)	16 m × 16 m	1	4	PR-9-16-0.4
				PR-9-14-1
				PR-9-16-1
Raft + 16 piles	14 m × 14 m	0.4	4	PR-16-14-0.4
(4 × 4 pile group)	16 m × 16 m	1	4	PR-16-16-0.4
				PR-16-14-1
				PR-16-16-1

each other in each pile are instrumented with strain gauges. Strain gauges are also positioned on the raft along the transverse and longitudinal sections. Load cells are placed in the PRF at the top and at the bottom of pile (P5) of capacities 100 Ton and 80 Ton, respectively. A hydraulic jack (1000 Ton capacity) has been used for applying load to the single pile and PRF. All instruments have been calibrated prior to testing. Dial gauges of 0.01 mm accuracy are used for measuring displacements. The detailed layout of the single pile and PRF and the detailed instrumentation of the piles and raft are shown in Fig. 4. Figure 4a shows the layout of the single pile and PRF. From Fig. 4a, it can be seen that the distance between the anchor piles is 3 m for a single pile load test and 5.34 m for a PRF load test. The diameter of both anchor piles and main piles is 0.4 m. The centre–centre distance of main pile from the anchor pile in the single pile load test is 2.1 m (more than 3 times the diameter of pile shaft). However, the centre–centre distance of main pile from the anchor pile in the PRF load test is 2 m (minimum distance that can be taken as per the code requirements [40]). Figure 4b shows the strain gauge instrumentation along the pile shaft. From Fig. 4b, it can be seen that five electrical strain gauges are installed in the reinforcement along the pile length. Figure 4c shows the strain gauge instrumentation along longitudinal and transverse directions of the raft. From Fig. 4c, it can be seen that the strain gauges in the reinforcements along longitudinal and transverse directions of the raft are attached at a distance of 0.3 m centre–centre from each other.

Table 5 Properties of piles and raft considered for the field study

Parameters	Pile	Raft
Material type	Concrete	Concrete
Length (L) in m	8	2.4
Raft width (B_r) in m	Nil	2.4
Raft thickness (t_r) in m	Nil	0.6
Diameter (d) in m	0.4	Nil
Young's modulus (E) in kN/m^2	29×10^6	29×10^6
Unit weight (Y) in kN/m^3	24	24

The ultimate load capacity (ULC) and the safe load capacity of the single pile are found out through the single pile load test. The calculated safe load of single pile from code [41] is found out to be 607 kN (60.7 Ton). The calculated ultimate load capacity of single pile from code [41] has been obtained from the following equation:

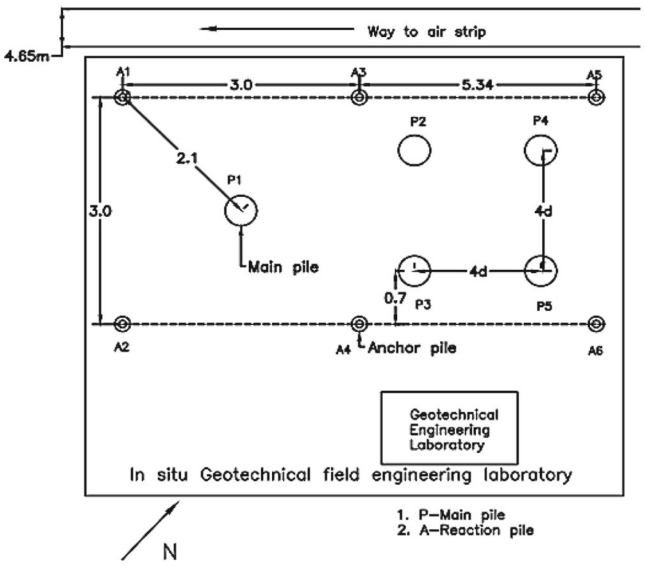

Diameter of main pile=0.4m
Diameter of anchor pile=0.4m
Distance between anchor piles=3m(For single pile load test)
Distance between anchor piles=5.34m(For piled– raft of spacing 4d)
Distance between group piles=4d=1.6m
Depth of anchor piles=10m
Depth of main piles=8m

(a)

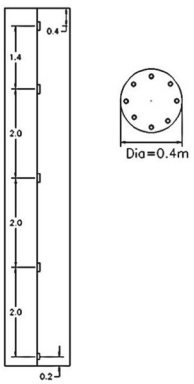

(b)

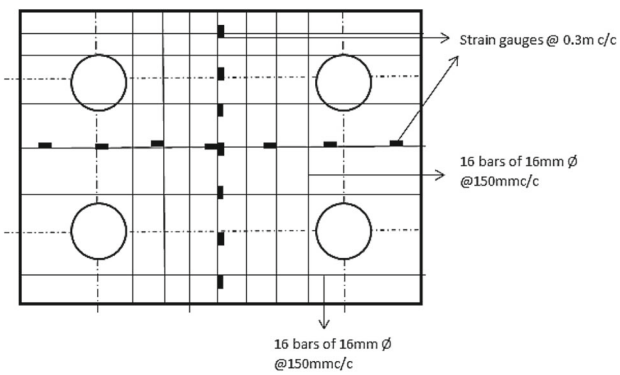

(c)

Fig. 4 **a** Layout of the single pile and PRF, **b** strain gauge instrumentation along the pile shaft, **c** strain gauge instrumentation along longitudinal and transverse directions of the raft

$$Q_u = A_p(0.5d\gamma N_\gamma + P_d N_q) + \sum_{i=1}^{n} K_i P_{di} \tan\delta_i A_{si} + A_P N_c c_P + \sum_{i=1}^{n} \alpha_i c_i A_{si} \quad (2)$$

where γ = effective unit weight of soil at pile tip in kN/m^3; N_γ and N_q = Bearing capacity factors depending on angle of internal friction at pile tip; P_d = effective overburden pressure at pile tip in kN/m^2; K_i = coefficient of earth pressure applicable for ith layer; P_{di} = effective overburden pressure for the ith layer in kN/m^2; δ_i = angle of wall friction between pile and soil for the ith layer; A_{si} = surface area of the pile shaft in the ith layer, in m^2; N_c = bearing capacity factor, taken as 9; A_p = cross-sectional area of pile toe in m^2; d = pile shaft diameter in m; α_i = adhesion factor for the ith layer depending on the consistency of soil; c_i = average cohesion for the ith layer in kN/m^2; c_P = average cohesion at pile tip in kN/m^2; and A_{si} = surface area of the pile shaft in the ith layer.

It is found from the above formula that the ultimate load capacity of a single pile is 1517 kN (151.7 Ton). Single pile load test has been conducted to determine the ultimate load capacity of single pile without considering time effect. Hence, the ultimate load capacity obtained from the single pile load test is an undrained capacity. By taking factor of safety as 2.5, safe load capacity of single pile is obtained as 607 kN. The calculated safe load capacity of the PRF comprising of 2 × 2 pile group is obtained by the sum of safe load-carrying capacity of raft and safe load-carrying capacity of single pile obtained from the single pile load test multiplied by the number of piles. The ULC of raft is obtained by the Meyerhof bearing capacity equation. The calculated safe load of the PRF has been found out to be 6131.1 kN (613.11 Ton). The load increment is 12 Ton (120 kN) in each step which is about 20% of the expected safe load capacity for the single pile load test. Figure 5a shows the load–settlement response from single pile load test. The ULC of the single pile is obtained as 94 Ton (940 kN) from the double tangent technique as presented in Fig. 5a. The safe load-carrying capacity of the single pile is obtained as 626.6 kN with respect to a settlement of 12 mm as per code [40].

For the PRF load test, axial loads have been applied starting from an increment of 10% till the calculated safe load. The settlement has been observed for a duration of 1 month for each increment of load applied. After the application of the safe load, the settlement is observed for a duration of 4 months. Hence, for PRF consisting of 2 × 2 pile group, the ultimate pile loads are based on drained loads. The properties of the soil strata, piles and raft for the numerical analysis are provided in Tables 2 and 5. The application of loads with respect to time in the PRF is presented in Table 6. The

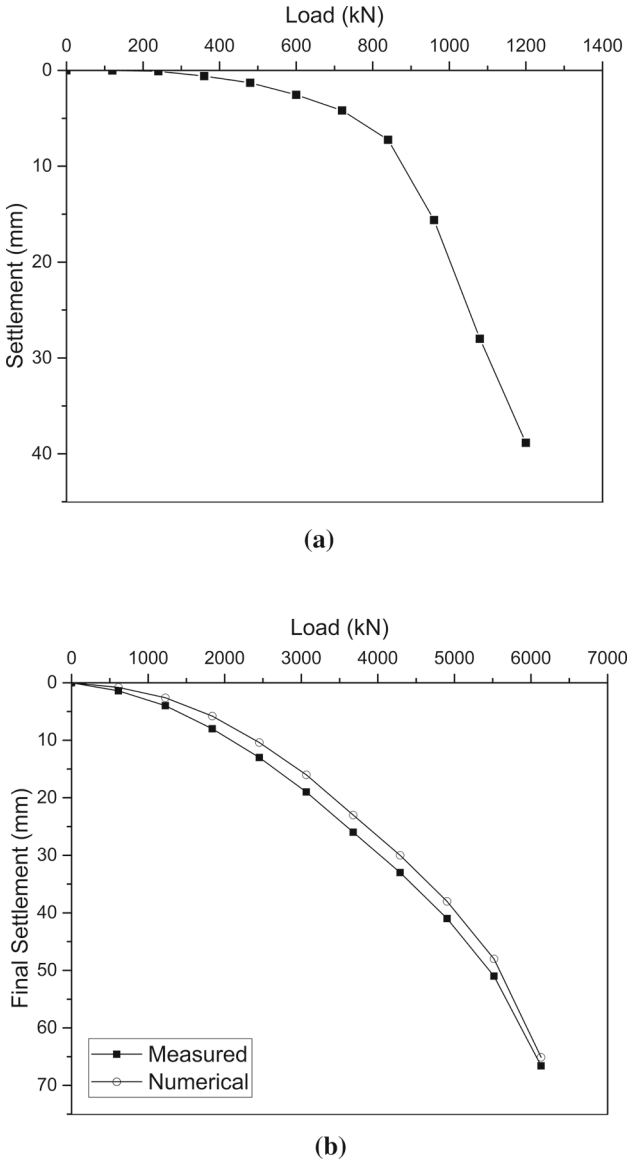

Fig. 5 **a** Load–settlement response from single pile load test, **b** final (consolidation) settlement of the PRF corresponding to the applied loads in each step

Young's modulus of the pile and raft material (E) is taken as 29 × 10^6 kN/m^2 (taking Young's modulus of steel (E_{st}) as 2 × 10^6 N/mm^2 and Young's modulus of concrete (E_c) as 25,000 N/mm^2, Young's modulus of RCC = $(E_{st}A_{st} + E_cA_c)/(A_s + A_c)$ = 29 × 10^6 kN/m^2).

The final (consolidation) settlement of the PRF corresponding to the applied loads in each step is shown in Fig. 5b. It is noticed that the initial section of the load–settlement curve is linear, while it becomes nonlinear afterwards. The applied loads vary in a nonlinear manner with the settlement. From the field load test, the final (consolidation) settlement corresponding to the safe load after 4 months has been obtained as 66.6 mm, whereas the final (consolidation)

Table 6 Application of loads with respect to time in the PRF

Load applied to the PRF (kN)	Time duration of the application of load (Month)
613.11 (10% of the safe load capacity)	0–1
1226.22 (20% of the safe load capacity)	1–2
1839.33 (30% of the safe load capacity)	2–3
2452.44 (40% of the safe load capacity)	3–4
3065.55 (50% of the safe load capacity)	4–5
3678.66 (60% of the safe load capacity)	5–6
4291.77 (70% of the safe load capacity)	6–7
4904.88 (80% of the safe load capacity)	7–8
5517.99 (90% of the safe load capacity)	8–9
6131.1 (100% of the safe load capacity)	9–13

settlement obtained in PLAXIS 3D is 65.11 mm. It can be concluded that the final (consolidation) settlement after a total time period of 13 months obtained by PLAXIS 3D is about 2.23% lesser than the measured settlement. The vertical displacement contour of PRF after 13 months can be seen in Fig. 6. From Fig. 6, it is observed that a final settlement of 65.11 mm is obtained by PLAXIS 3D after a total time period of 13 months. The settlement–time response of PRF for all the increments of loading applied for their respective time periods is shown in Fig. 7a. It is a typical figure describing the time-dependent nature shown by every PRF configurations considered in the study. The settlement–time curve consists of three portions such as (i) linear portion or nonlinear portion depicting elastic settlement up to the time of load application, (ii) middle portion depicting a power law variation of settlement with time and (iii) final portion depicting a logarithmic variation of settlement with time. The linear or nonlinear potion depicts the immediate or elastic settlement occurred within a short span with no volume change in soil. The middle portion and the final portion curves represent the consolidation settlement due to the elastoplastic deformation of soil and dissipation of excess pore water pressure from the soil.

The axial load distribution along the pile shaft has been calculated from the following equation:

$$q_i = \epsilon_i E A_i \tag{3}$$

where q_i = Pile axial load at the location of strain gauge; E = Modulus of elasticity of pile material taken as 29E6 kN/m^2; and A_i = Cross sectional area at the location of strain gauge. Figure 7b shows the optimum axial load distribution along the pile shaft of pile P5 for various load increments that has been applied to the piled raft over the period of 13 months. The intensity of load distribution along the shaft decreases with increase in depth up to 6 m, and it is minimal thereafter. The load distribution remains constant at the bottom end of

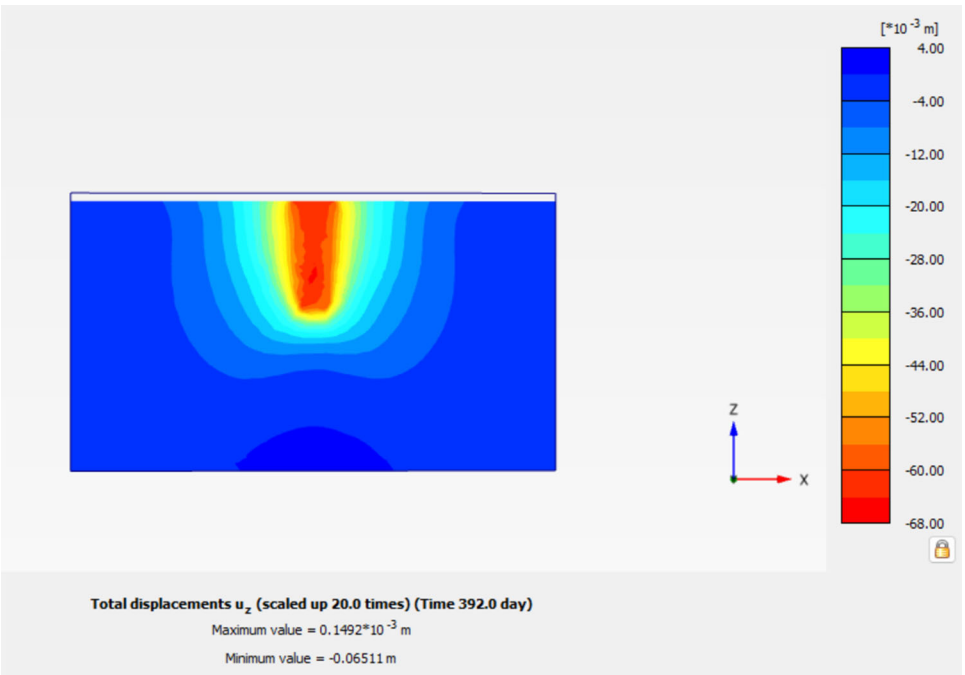

Fig. 6 Vertical displacement contour of PRF after 13 months

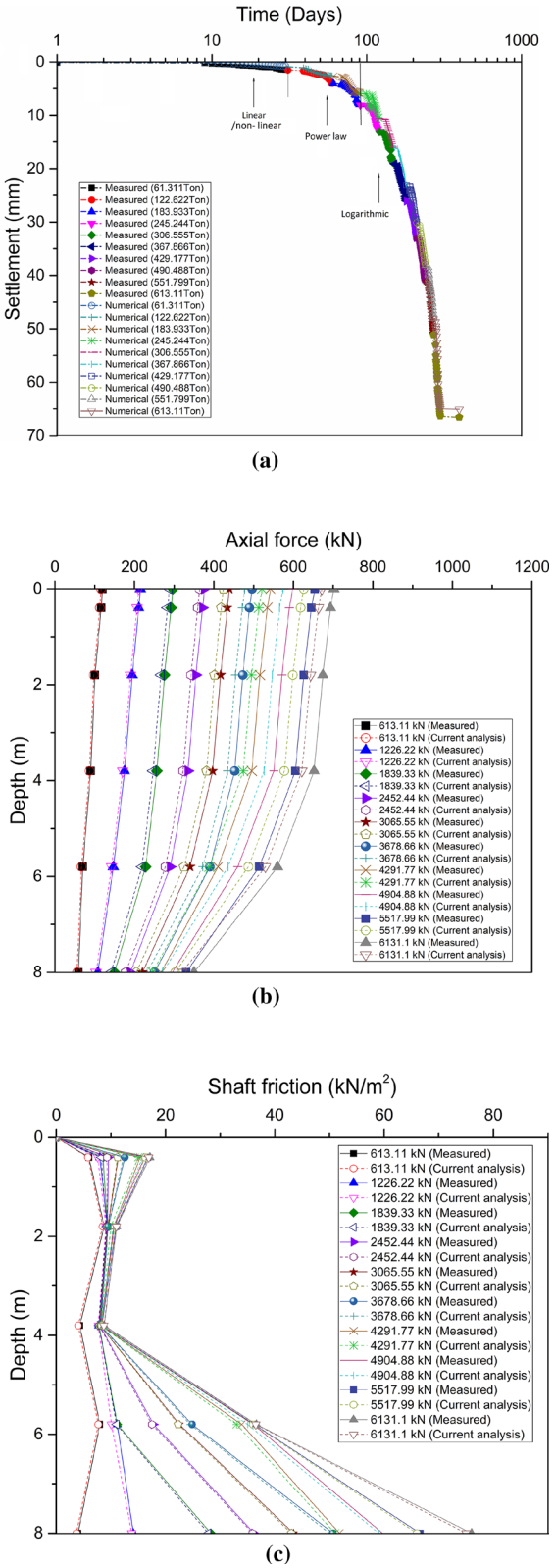

Fig. 7 **a** Settlement–time response of PRF for all the increments of loading applied for their respective time periods, **b** optimum axial load distribution along the pile shaft of pile P5 for various load increments that has been applied to the piled raft over the period of 13 months, **c** shaft friction along the pile shaft (P5) for all the load increments over a period of 13 months

the pile. Also, as the intensity of axial load increases, the load distribution along the pile shaft increases. The measured results have been compared with the current analysis, and it is found out that the measured axial loads are about 2–5% higher than the axial loads obtained by the current analysis.

The shaft friction along the pile shaft has been calculated as per the equation given below:

$$f_{ij} = \frac{(q_j - q_i)}{S_{ij}} \tag{4}$$

where f_{ij} denotes the average shaft friction between stations i and j; q_j and q_i denote axial load at the location of strain gauges j and i, respectively; and S_{ij} denotes surface area of the pile between stations i and j. Figure 7c shows the shaft friction along the pile shaft (P5) for all the load increments over a period of 13 months. It is observed that the shaft friction increases after a depth of 3.8 m till 8 m. It is maximum at the end of the pile, i.e. at 8 m. The shaft friction starting from depth 3.8–8 m is larger than the shaft friction at shallow depths. Also, as the intensity of load increases, the shaft friction along the pile shaft increases. The measured results have been compared with the current analysis, and it has been found that the measured shaft frictions are about 1–4% higher than the shaft frictions obtained by the current analysis.

5.2 Validation with the Numerical Results Reported by Cho et al. [8]

The vertical average settlements (Δ_{avg}) reported from the results of Cho et al. [8] for point loading condition in case of soft clay and stiff clay have been validated. The average settlement can be obtained from Eq. (29). The PRF is considered to be embedded in soft clay and stiff clay conditions. The ground water table is considered to be at the ground level. Single drainage condition has been considered, and consolidation effect has been neglected in the analysis. A raft size of 10 m × 10 m × 1 m and a 3 × 3 pile group configuration has been considered. The diameter and length of piles are taken as 0.5 m and 8 m, respectively. The spacing between the piles is taken as three times the diameter of the pile. The properties of the soil strata, raft and piles adopted from Cho et al. [8] are shown in Table 7. The Mohr–Coulomb constitutive model has been considered for the modelling of soft clay, stiff clay and the bearing layer. The bearing layer has been placed beneath the clay layer as mentioned [8]. The load–average settlement behaviour obtained from the current finite element analysis has been compared with that obtained by the reported results [8]. The load–average settlement curve for validation with Cho et al. [8] is presented in Fig. 8. An overall error of 2.31% and 2.94% has been obtained in case of PRF embedded in soft clay and stiff clay, respectively, which

Table 7 Properties of the soil strata, raft and piles adopted from Cho et al. [8]

Material Parameters	Soil properties			Concrete properties	
	Soft clay	Stiff clay	Bearing layer	Pile	Raft
Thickness of soil layer (m)	20	20	4	–	–
Cohesion, c' (Mpa)	3	20	0.1	–	–
Elasticity modulus of soil, E_s (Mpa)	5	45	500	–	–
Elasticity modulus of concrete, E_c (Mpa)	–	–	–	12,500	30,000
Friction angle, ϕ' (Degree)	20	20	45	–	–
Coefficient of earth pressure at rest, K_o	0.65	0.65	0.5	–	–
Poisson's ratio of soil, ν_s	0.3	0.3	0.3	–	–
Poisson's ratio of concrete, ν_c	–	–	–	0.25	0.2
Unit weight of soil, Y_s (kN/m^3)	18	19	20	–	–
Unit weight of concrete, Y_c (kN/m^3)	–	–	–	25	25

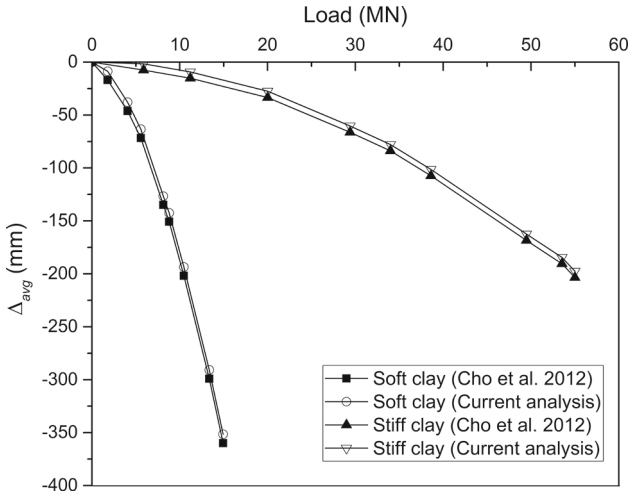

Fig. 8 Load–average settlement curve for validation with Cho et al. [8]

indicates a good agreement between the current analysis and reported results. Hence, it is verified that the validations prove the reliability of the numerical model, and hence, it can be used for further analyses.

6 Results and Discussion

First the load-carrying capacity of the foundation system is determined by performing only plastic analysis. Then, consolidation analysis of the foundation systems is performed by applying the load in increments of 10% of ultimate load till the ultimate load. The settlement is observed for a period of 1 month for each increment of loading and a period of 1 year for the ultimate load capacity (ULC). The parametric cases mentioned in Table 4 have been analysed for the load–settlement response, settlement–time response, influence of load sharing behaviour, interaction effects and factor of safety on consolidation settlement of PRFs.

6.1 Influence of the Size of Un-Piled Raft (UR), Diameter and Number of Piles in PRF on the Settlement Time Curve

The load–settlement curves of the URs (UR-14 and UR-16) and PRFs (PR-1-14-0.4, PR-1-16-0.4, PR-1-14-1, PR-1-16-1, PR-4-14-0.4, PR-4-16-0.4, PR-4-14-1, PR-4-16-1, PR-9-14-0.4, PR-9-16-0.4, PR-9-14-1, PR-9-16-1, PR-16-14-0.4, PR-16-16-0.4, PR-16-14-1 and PR-16-16-1) have been obtained. Figure 9a shows the load–settlement curves of the URs and PRFs having raft width 16 m. Figure 9b shows the load–settlement curves of the URs and PRFs having raft width 14 m. For example, UR-14 refers to un-piled raft having size 14 m × 14 m and PR-1-14-0.4 refers to PRF consisting of single pile having raft size as 14 m × 14 m and pile diameter as 0.4 m. Only plastic analysis has been performed to determine the load-carrying capacity of the foundation systems. The ultimate load capacities (ULCs) of the various configurations of URs and PRFs are mentioned in Table 8. The ULCs are obtained from the double tangent technique. From Table 8, it has been observed that PR-16-16-1 has the highest ULC among all the PRFs. The ULC of UR-16 is about 11.11% higher than UR-14. The settlement–time curves of URs and PRFs having raft width 16 m are presented in Fig. 9c. The settlement–time curves of URs and PRFs having raft width 14 m are presented in Fig. 9d. For the time-dependent settlement, consolidation analysis is performed by applying the load in increments of 10% of ULC till the ULC is reached. The settlement is observed for 1 month for each increment of loading and a period of 1 year for the ULC. The settlements observed at the end of 1 month for each increment of loading and at the end of 1

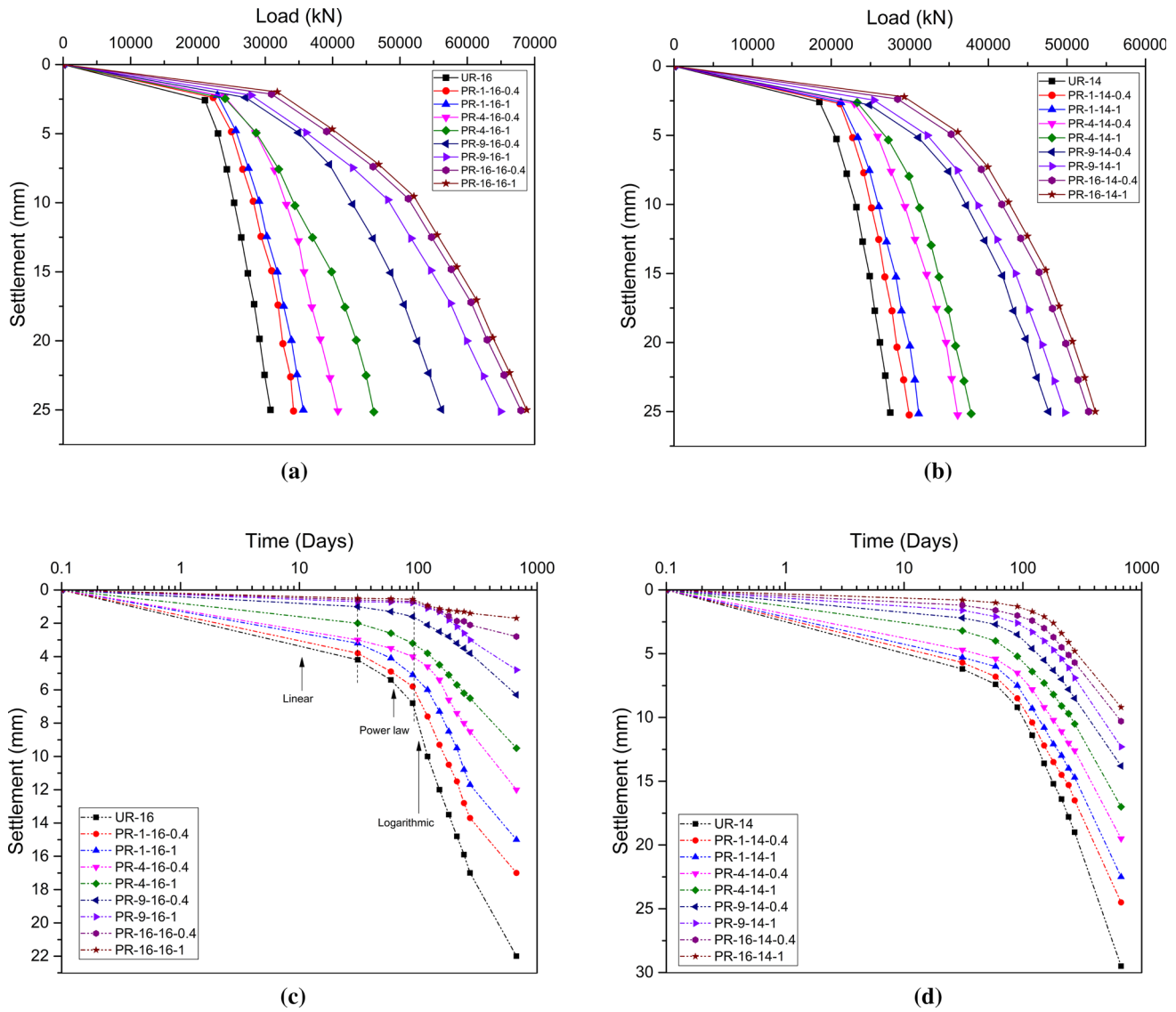

Fig. 9 **a** Load–settlement curves of the URs and PRFs having raft width 16 m, **b** load–settlement curves of the URs and PRFs having raft width 14 m, **c** settlement–time curves of URs and PRFs having raft width 16 m, **d** settlement–time curves of URs and PRFs having raft width 14 m

year after the ULC has been applied are plotted in Fig. 9c, d. The long-term (consolidation) settlement shows noticeable nonlinearity as pronounced from the settlement–time plots. The final settlement including the immediate and consolidation settlements obtained at the end of 22 months is about 240–1050% more than the immediate settlement obtained at the end of 1 month for all the foundation systems considered. The settlement obtained at the end of 9 months corresponding to 90% of the ULC is about 22–91% lesser than the final settlement obtained at the end of 22 months for all the foundation systems considered. Increase in the size of UR leads to increase in the load capacity. It can be described by the fact that the relative stiffness of raft is increased as the size of raft is increased from 14 m × 14 m to 16 m × 16 m which leads to sustain more load. As the number of piles (n) increases in the PRF, the load capacity increases. This can be explained from the fact that the stiffness of PRF is enhanced by an increased number of piles which results in the increased load capacity. The load capacity of the PRF is increased by the increase in the pile diameter. This increase in the load capacity might be because of the increase in stiffness and surface area of the piles in the PRF. As the load-carrying capacity is increased, the final settlement is decreased. The final (consolidation) settlement is decreased with the increase in the raft size, number of piles and pile diameter of the PRF.

Table 8 Ultimate load capacities (ULCs) of the various configurations of URs and PRFs

Type of foundation	Ultimate load capacity (kN)
UR-14	21,600
UR-16	24,000
PR-1-16-0.4	28,000
PR-1-16-1	30,000
PR-4-16-0.4	32,000
PR-4-16-1	35,000
PR-9-16-0.4	43,000
PR-9-16-1	48,000
PR-16-16-0.4	50,000
PR-16-16-1	51,000
PR-1-14-0.4	24,000
PR-1-14-1	26,000
PR-4-14-0.4	29,000
PR-4-14-1	30,000
PR-9-14-0.4	38,000
PR-9-14-1	39,000
PR-16-14-0.4	41,000
PR-16-14-1	42,000

6.2 Evaluation of Long-Term Interaction Factors and LDC

The load capacity of PRF can be mentioned in terms of load capacity of un-piled raft and pile group as depicted by the formula:

$$Q_{pr} = Q_{UR} + Q_{gp} = \beta_{rp} Q_{UR} + \beta_{pr} \beta_{pp} \sum_{n=1}^{n} Q_{sp} \tag{5}$$

where Q_{UR} denotes the load-carrying capacity of un-piled raft; Q_{gp} denotes the load capacity of pile group; n denotes the number of piles beneath the raft; Q_{sp} denotes the load capacity of single pile; β_{rp} denotes the raft–pile interaction factor; β_{pr} denotes the pile–raft interaction factor; and β_{pp} denotes the pile–pile interaction factor. The evaluation of the long-term interaction factors is given in the following sections.

6.2.1 Pile–pile (P–P) Interaction Factor (β_{pp})

If piles are situated close to each other, the stress fields are superposed. The settlement response of the pile varies due to the superpositioning of the stress fields. This variation in the settlement response is caused due to the interaction between piles (pile–pile interaction). There is an amount of additional settlement occurring in a single pile due to the presence of adjacent piles. The pile–pile interaction factor can be written as:

$$\beta_{pp} = \frac{Q_{gp}}{n Q_{sp}} \tag{6}$$

where Q_{gp} denotes the load capacity of pile group; n denotes the number of piles beneath the pile cap; and Q_{sp} denotes the load capacity of single pile.

In the current context, the load capacities of single piles (SPs) and pile groups (GPs) are calculated separately. Pile groups having the same pile group configurations and dimensions in case of PRFs have been considered. The raft dimensions remain same as the pile cap dimensions considered for the pile group and single pile. The pile dimensions (length and diameter) in case of PRF remain same in case of GP and SP. For example, corresponding to PR-4-16-0.4, GP-4-16-0.4 has been considered where GP represents the group pile, 4 represents the number of piles, 16 represents the pile cap size of 16 m × 16 m, and 0.4 represents the pile diameter of 0.4 m. In this study, for the estimation of long-term β_{pp}, the following steps are followed for the analysis:

i. The load-carrying capacity of the foundation systems (SPs and GPs) is determined by providing incremental compressive loads at the centre of the pile cap. The ULC is obtained by the double tangent technique. Only plastic analysis is performed.
ii. Analyses are performed considering time effect. Vertical loading at the centre of pile cap has been applied in increments of 10% of the ULC of the SP/GP in each step till the ULC is reached. For each increment of loading, settlement is observed for 1 month but after application of ULC, the settlement is observed for 1 year. Consolidation analysis is carried out at each step of loading.
iii. The load taken by the group piles (Q_{gp}) and single pile (Q_{sp}) for each increment of loading at the end of 1 month and at the end of 1 year after the application of ULC has been calculated. The final (consolidation) settlements obtained at the end of 1 month for each increment of loading and at the end of 1 year after the application of ULC are noted.
iv. β_{pp} is obtained from Eq. (6), and it has been plotted against the final settlements obtained.

Figure 10 shows a typical figure of β_{pp} with final (consolidation) settlement corresponding to each increment of loading applied till the ultimate load for GP-4-14-0.4 and SP having 0.4 m diameter. It has been observed that β_{pp} value decreases as the final settlement increases. However, the decrease is very nominal of about 1%. It has been observed from analysis that for all the configurations of GPs and SPs considered, β_{pp} is nearly equal to 1 or equal to 1. Hence,

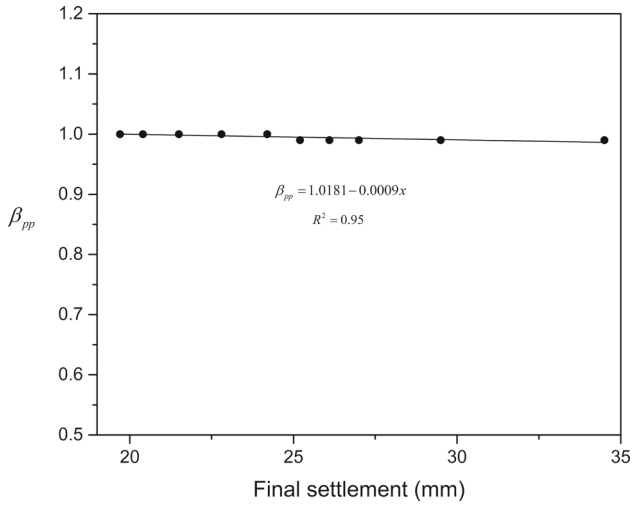

Fig. 10 β_{pp} with final (consolidation) settlement corresponding to each increment of loading applied till the ultimate load for GP-4-14-0.4 and SP having 0.4 m diameter

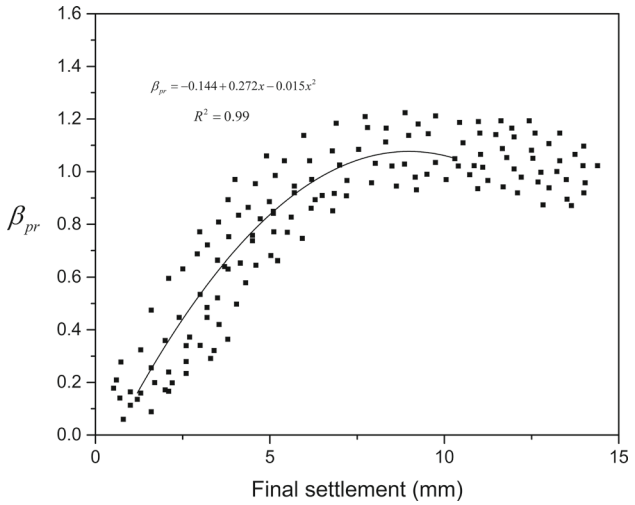

Fig. 11 Variation of β_{pr} with final (consolidation) settlement corresponding to each increment of loading applied till the ultimate load for all the configurations of PRFs considered

β_{pp} is considered as 1 in the present study as also confirmed elsewhere [42].

6.2.2 Pile–raft (P–R) Interaction Factor (β_{pr})

The settlement response of pile in a PRF is unlike single pile or pile group (PG) because of the existence of raft. If a raft is positioned over a PG, then the load–settlement behaviour of the foundation is changed unlike a pile group. This change in the load–settlement behaviour can be attributed as pile–raft interaction. The P–R interaction factor can be expressed as:

$$\beta_{pr} = \frac{Q_{gp-pr}}{Q_{gp}} \tag{7}$$

where Q_{gp-pr} denotes the load capacity of group piles in a PRF. β_{pr} can affect the pile response in both positive and negative aspects. The positive aspect is the increase in skin resistance due to increase in the confining pressure of soil due to the raft presence. The negative aspect is the lesser mobilization of skin resistance.

In this study, for the estimation of long-term β_{pr}, the following steps are followed for the analysis:

v. The load-carrying capacity of the foundation systems (PRFs and GPs) is determined by providing incremental compressive loads at the centre of the raft/pile cap. The ULC is obtained by the double tangent technique. Only plastic analysis is performed.
vi. Analyses are performed considering time effect. Vertical loading at the centre of raft/pile cap has been applied in increments of 10% of the ULC of the PRF/GP in each step till the ULC is reached. For each increment of loading, settlement is observed for 1 month but after application of ULC, the settlement is observed for 1 year. Consolidation analysis is carried out at each step of loading.
vii. The load taken by the group piles in the PRF (Q_{gp-pr}) and group piles (Q_{gp}) for each increment of loading at the end of 1 month and at the end of 1 year after the application of ULC has been calculated. The final (consolidation) settlements obtained at the end of 1 month for each increment of loading and at the end of 1 year after the application of ULC are noted.
viii. β_{pr} is obtained from Eq. (7), and it has been plotted against the final settlements obtained.

Figure 11 denotes variation of β_{pr} with final (consolidation) settlement corresponding to each increment of loading applied till the ultimate load for all the configurations of PRFs considered. It is observed that both positive and negative aspects are there due to the pile–raft interaction effect. The β_{pr} values less than unity replicate the negative aspect of pile–raft interaction, while the β_{pr} values above unity replicate the positive aspect of pile–raft interaction. It is observed that β_{pr} increases with the increasing magnitude of final settlement. At higher magnitude of settlement, β_{pr} becomes more than unity. The lower value of β_{pr} indicates early mobilization of shaft (skin) friction of pile generating lesser contact pressure between soil and raft. At larger settlement levels, the load-carrying capacity of piles in a PRF becomes almost equal to the load-carrying capacity of group piles. It is observed that a similar response has been shown by all the PRF configurations. As the number of piles increases, there is very less influence on β_{pr} which can be verified from the polynomial expression obtained from the best fitted curve as

follows:

$$\beta_{pr} = -0.144 + 0.272x - 0.015x^2 \tag{8}$$

where x is the final settlement (mm). The R^2 value for the above equation is 0.99. β_{pr} initially increases up to a final settlement of 9 mm and then gradually decreases due to the further settlement of raft. The highest value of β_{pr} obtained is 1.2. It can also be concluded that β_{pr} depends on the number of piles (n), diameter of piles (d), width of raft (B_r) and consolidation settlement (x). Hence, β_{pr} can be written as a function of all these variables as given by the equation:

$$\beta_{pr} = \mathrm{f}\,(n,\ x/d,\ B_r/d) \tag{9}$$

The final (consolidation) settlement is considered in the normalized form as x/d. Width of the raft is normalized as B_r/d. Using multiple linear regression analysis, a generalized prediction equation has been obtained using the results obtained from the analysis as:

$$\beta_{pr} = 0.518 - 0.038n + 8.406\frac{x}{d} + 0.0205\frac{B_r}{d} \tag{10}$$

where the units of x, d and B_r are taken in 'm'. It has been observed that the percentage difference in β_{pr} values obtained by Eq. (8) and Eq. (10) is ± 15%. The relation of β_{pr} with the final (consolidation) settlement can be helpful for the idealization of β_{pr} for different PRF configurations in low plasticity clay and intermediate plasticity clay.

6.2.3 Raft–pile (R–P) Interaction Factor (β_{rp})

If a certain number of piles (n) are present beneath the raft, then β_{rp} comes into picture. The load–settlement response of the raft in PRF is different than the UR because of the presence of piles underneath the raft. The shaft friction of pile mobilizes gradually, and the neighbouring soil moves in the downward direction which leads to a lesser contact pressure between the soil and the raft. This causes the load capacity of the raft to reduce when subjected to a load. The change in the load–settlement behaviour of raft in the PRF can be attributed as raft–pile interaction factor (β_{rp}) and can be given as:

$$\beta_{rp} = \frac{Q_{r-pr}}{Q_{UR}} \tag{11}$$

where Q_{r-pr} denotes the load-carrying capacity of raft in a PRF and Q_{UR} denotes the load-carrying capacity of un-piled raft.

From Eqs. (11) and (18), β_{rp} can be written as:

$$\beta_{rp} = \frac{1}{1-\alpha_{pr}} - \frac{\beta_{pr}}{\psi} \tag{12}$$

where $\psi = \frac{Q_{UR}}{Q_{gp}}$.

β_{rp} is evaluated by using both the equations where Eq. (11) includes the results obtained numerically (PLAXIS 3D) and Eq. (12) includes the results from the predicted equations. In this study, for the estimation of long-term β_{rp}, the following steps are followed:

i. The load-carrying capacity of the foundation systems (PRFs and URs) is determined by providing incremental compressive loads at the centre of the raft. The ULC is obtained by the double tangent technique. Only plastic analysis is performed.
ii. Analyses are performed considering time effect. Vertical loading at the centre of raft has been applied in increments of 10% of the ULC of the PRF/UR in each step till the ULC is reached. For each increment of loading, settlement is observed for 1 month but after application of ULC, the settlement is observed for 1 year. Consolidation analysis is carried out at each step of loading.
iii. The load taken by the raft in the PRF (Q_{r-pr}) and unpiled raft (Q_{UR}) for each increment of loading at the end of 1 month and at the end of 1 year after the application of ULC has been calculated. The final (consolidation) settlements obtained at the end of 1 month for each increment of loading and at the end of 1 year after the application of ULC are noted.
iv. β_{rp} is obtained from Eq. (9), and it has been plotted against the final settlements obtained.

Figure 12a denotes variation of β_{rp} with final (consolidation) settlement corresponding to each increment of loading applied till the ultimate load for all the configurations of PRFs considered. From Fig. 12a, it has been observed that there is an initial decrease in β_{rp}. It is due to the lesser contact pressure among the soil and the raft. Afterwards, the β_{rp} value increases because of raft starting to take load. The following polynomial equation has been deduced by fitting the curve:

$$\beta_{rp} = 2.438 - 0.727x + 0.096x^2 - 0.003x^3 \tag{13}$$

where x is the final (consolidation) settlement. The R^2 value for the above equation is 0.98, and the standard error is 0.02. β_{rp} value decreases up to a final settlement of 5 mm and increases thereafter. It is due to the further settlement of raft because of the incremental vertical loading. The lowest and highest values of β_{rp} are 0.5 and 1.8 corresponding to the final settlement level of 15.3 mm and 0.5 mm, respectively. β_{rp} decreases initially because of the fast mobilization of load capacity of piles at the initial increments of loading which leads to a lesser pressure surrounding the contact area between the soil and the raft near the piles. β_{rp} increases afterwards because of the raft starting to take load as the final settlement increases. The predicted β_{rp} results are mapped

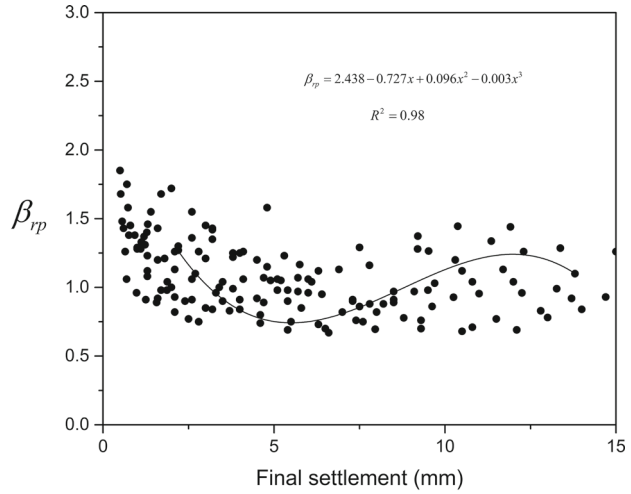

Fig. 12 **a** Variation of β_{rp} with final (consolidation) settlement corresponding to each increment of loading applied till the ultimate load for all the configurations of PRFs considered**, b** calculated β_{rp} versus predicted β_{rp}

with respect to the numerical results. The calculated β_{rp} versus predicted β_{rp} is presented in Fig. 12b. It can be observed that the numerical results express good compliance with the predicted results having an error of 1–5%.

As the number of piles in the PRF increases, load-carrying capacity of PRF increases, and the final settlement decreases. The β_{rp} increases due to the increase in number of piles, pile diameter and raft size. Hence, β_{rp} can be written as a function of number of piles (n), diameter of piles (d), width of raft (B_r) and consolidation settlement (x). Hence, β_{rp} can be expressed as:

$$\beta_{rp} = \mathrm{f}\,(n,\ x/d,\ B_r/d) \tag{14}$$

Using multiple linear regression analysis, a generalized equation in terms of various parameters has been obtained using the results obtained from the analysis as:

$$\beta_{rp} = 1.271 + 0.0114n - 8.36\frac{x}{d} - 0.0084\frac{B_r}{d} \tag{15}$$

It has been observed that the percentage difference in the β_{rp} values obtained by Eqs. (11) and (15) is ± 10%. The relation of β_{rp} with the final (consolidation) settlement can be helpful for the idealization of β_{rp} for different PRF configurations in low plasticity clay and intermediate plasticity clay.

6.2.4 LDC (ζ)

ζ can be expressed as [22]:

$$\zeta = \frac{Q_{pr}}{Q_{UR} + Q_{gp}} \tag{16}$$

The load distribution coefficient (ζ) can also be written as:

$$\zeta = \frac{\psi\beta_{rp} + \beta_{pr}}{1 + \psi} \tag{17}$$

The interaction factors and ζ for the PRFs have been evaluated for the final (consolidation) settlement obtained after 22 months. The pile–raft interaction factor (β_{pr}), raft–pile interaction factor (β_{rp}) and load distribution coefficient (ζ) considering different PRF configurations are presented in Table 9. A range for β_{pr}, β_{rp} and ζ can be obtained from Table 9 considering different PRF configurations. β_{pr}, β_{rp} and ζ vary from 0.24 to 1.94, 0.4 to 1.98 and 0.39 to 1.949, respectively. The values indicate that β_{pr} imposes a negative influence on the ULC of the PRF. The presence of raft in a PRF minimizes the corresponding displacement of piles and neighbouring soils. It results in the decrease in mobilization of piles in PRF rather than pile foundation. β_{rp} has both positive and negative influence on load capacity and settlement aspects of PRF. ζ has a negative influence on PRF as the ultimate load-carrying capacity of PRF is lesser than the sum of load-carrying capacity of raft and pile group. An appropriate estimation of the interaction factors is necessary prior to the design of PRF because of such negative and positive effects of the interaction factors and keeping in view the consolidation (final) settlement behaviour of PRF.

6.3 Variation of Load Sharing Ratio (LSR) (α_{pr}) with Final Settlement

The LSR (α_{pr}) has been obtained equal to the proportion of load taken by the piles to the total load taken by the PRF. α_{pr}

Table 9 Pile–raft interaction factor (β_{pr}), raft–pile interaction factor (β_{rp}) and load distribution coefficient (ζ) considering different PRF configurations

Model	n	B_r	D	β_{pr}	β_{rp}	ζ
PR-1-14-0.4	1	14	0.4	0.24	0.4	0.39500538
PR-4-14-0.4	4	14	0.4	1.04	0.62	0.78777875
PR-9-14-0.4	9	14	0.4	1.27	0.67	1.04818224
PR-16-14-0.4	16	14	0.4	1.45	1.02	1.31527897
PR-1-16-0.4	1	16	0.4	0.7	1.26	1.11518065
PR-4-16-0.4	4	16	0.4	1.51	1.33	1.41531792
PR-9-16-0.4	9	16	0.4	1.91	1.39	1.75148699
PR-16-16-0.4	16	16	0.4	1.93	1.96	1.93712871
PR-1-14-1	1	14	1	0.44	1.06	0.97749049
PR-4-14-1	4	14	1	1.47	1.13	1.28906178
PR-9-14-1	9	14	1	1.63	1.38	1.54278938
PR-16-14-1	16	14	1	1.67	1.95	1.7543714
PR-1-16-1	1	16	1	0.86	1.48	1.2758263
PR-4-16-1	4	16	1	1.68	1.36	1.53207547
PR-9-16-1	9	16	1	1.92	1.42	1.79252625
PR-16-16-1	16	16	1	1.94	1.98	1.94924188

can be given as:

$$\alpha_{pr} = \frac{Q_p}{Q_{pr}} = \frac{Q_p}{Q_r + Q_p} = 1 - \frac{Q_r}{Q_{pr}} \tag{18}$$

where Q_p denotes sum of loads taken by piles; Q_{pr} denotes total applied load to the PRF; and Q_r denotes load taken by the raft in the PRF.

It has been observed that the piles carried most of the applied load during the initial loading phase. The proportion of load taken by piles decreased slowly as the settlement increased [23]. The piles carried most of the applied load during the initial incremental loading phase due to a possible low contact between the base of raft and soil surface. The load sharing ratios have been calculated for each foundation type corresponding to each increment of loading at the end of 1 month and at the end of 1 year after the application of ULC. The load sharing ratio value has been taken with respect to the final settlement obtained for each increment of loading. If the raft width increases, then the soil confinement also increases which increases the pile mobilization, hence enhancing the load capacity of PRF. The increase in number of piles in PRF leads to support more load, thereby increasing α_{pr} value. The variation of load sharing ratio with the final settlement for all the increment of loadings applied for all the foundation types is plotted in Fig. 13a. From Fig. 13a, it is observed that α_{pr} value is high, i.e. 0.5–0.9 in the settlement range of 0.5–12.5 mm, and then, it decreases in a nonlinear manner as the final settlement increases. It has been observed that as the width of raft increased, α_{pr} also increased. If the raft width increases, then the soil confinement also increases which increases the pile mobilization, hence enhancing the load capacity of PRF. α_{pr} is also increased with the rise in the number of piles and pile diameter in the PRF as a greater number of piles and a larger pile diameter will help to support more load. As the number of piles, pile diameter and width of raft increases, α_{pr} increases by about 34–48%, 6–19% and 11–20%, respectively. The best fit has been obtained, and a generalized polynomial expression has been articulated:

$$\alpha_{pr} = 1.007 - 0.074x + 0.00175x^2 \tag{19}$$

where x is the final settlement obtained for each increment of loading. The R^2 value for the above equation is 0.98. The results obtained using Eq. (19) has been then authenticated with reference to the calculated α_{pr} values. The calculated α_{pr} versus predicted α_{pr} is presented in Fig. 13b. It is evident that Fig. 13b acquires a satisfactory interrelationship between LSR and final settlement having an ordinary error of 0.09. Figure 13c denotes a typical figure depicting the variation of α_{pr} values with time and final settlement for PR 4-14-0.4. It is observed from Fig. 13c that as the time increases for each load increment, the final settlement increases, while the α_{pr} value decreases for all the PRFs considered. It has been observed that α_{pr} value depends on the number of piles (n), diameter of piles (d), width of raft (B_r), final (consolidation) settlement (x) and time taken (t). Hence, α_{pr} can be expressed as:

$$\alpha_{pr} = f\,(n,\, x/d,\, B_r,\, t) \tag{20}$$

Using multiple linear regression analysis, a generalized equation in terms of various parameters has been obtained using the results obtained from the analysis as:

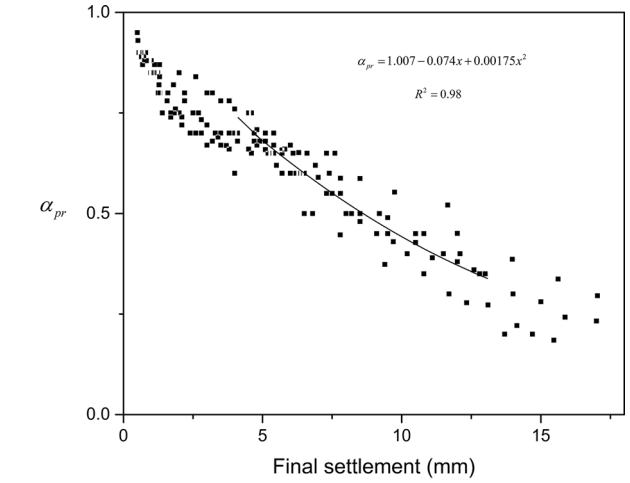

(a)

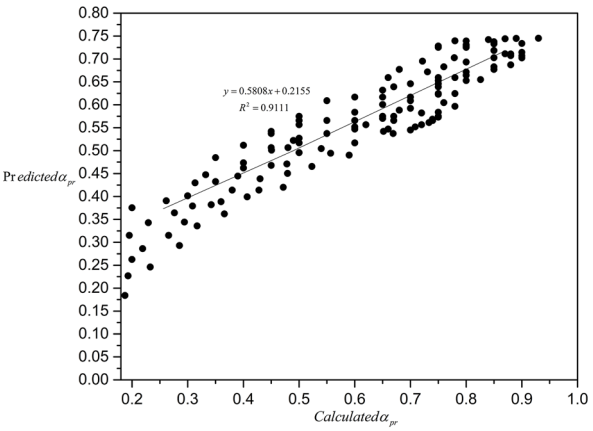

(b)

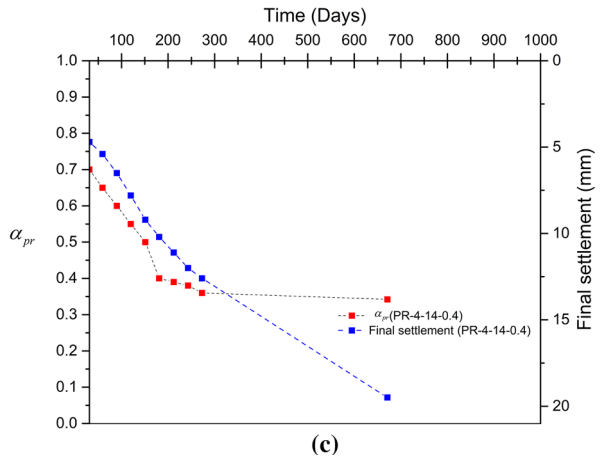

(c)

Fig. 13 **a** Variation of load sharing ratio with the final settlement for all the increment of loadings applied for all the foundation types, **b** calculated α_{pr} versus predicted α_{pr}, **c** variation of α_{pr} values with time and final settlement for PR 4-14-0.4

$$\alpha_{pr} = -0.02918 + 0.014437n - 8.74901\frac{x}{d} + 0.04633B_r - 0.00025t \quad (21)$$

where units of diameter of piles (d) and width of raft (B_r) are taken in 'm', and time (t) is taken in 'days'. Using Eq. (21), α_{pr} values have been cross checked with the calculated analysis values and it has been observed that the difference in values is ± 20%. Hence, Eq. (21) can be used to the α_{pr} values in case of PRFs subjected to incremental compressive loading considering time effect in case of low plasticity clay and intermediate plasticity clay (Kanpur soil).

6.4 Prediction Model for PRF

A model has been predicted based on the numerical analyses for the estimation of ULC of PRF. The ULC of PRF can be obtained by utilizing the interaction factors calculated in the preceding section. The ULC of PRF can thus be expressed as:

$$Q_{\text{pr, ult}} = \frac{\psi\beta_{rp} + \beta_{pr}}{1 + \psi}\left(Q_{\text{UR, ult}} + Q_{\text{gp, ult}}\right) \quad (22)$$

The piles in a pile group ensure a proper factor of safety (FS) in case of failure. Selecting a pile group containing a greater number of piles mostly leads to very small amount of settlement and is not cost effective. For these reasons, design of PRFs should be done based on overall FS of the PRF.

The overall FS of PRF can be estimated in terms of FS of the pile group (FS_{gp}) and UR (FS_{UR}).

$$FS_{UR} = \frac{Q_{UR,\,ult}}{Q_a} \quad (23)$$

$$FS_{gp} = \frac{Q_{gp,\,ult}}{Q_a} \quad (24)$$

$$FS_{pr} = \frac{Q_{pr,ult}}{Q_a} \quad (25)$$

where Q_a is the applied load.

Equation (16) can be written in terms of FS as:

$$\zeta_{pr} = \frac{Q_{pr,ult}}{Q_{UR,ult} + Q_{gp,ult}} = \frac{FS_{pr}}{FS_{UR} + FS_{gp}} \quad (26)$$

Thus, FS of PRF can be written by combining Eq. (23) and Eq. (26);

$$FS_{pr} = \zeta_{pr}(FS_{UR} + FS_{gp}) = \frac{\psi\beta_{rp} + \beta_{pr}}{1 + \psi}(FS_{UR} + FS_{gp}) \quad (27)$$

In Fig. 14a, the factor of safety of PRF (PR-9-16-1) against the final (consolidation) settlement (for all the increments of

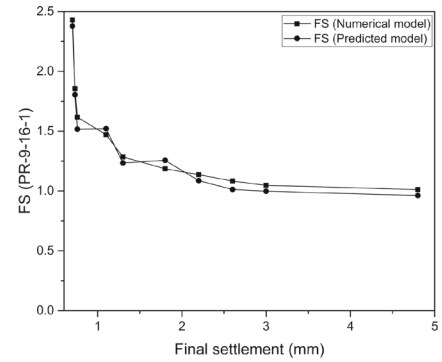

(a)

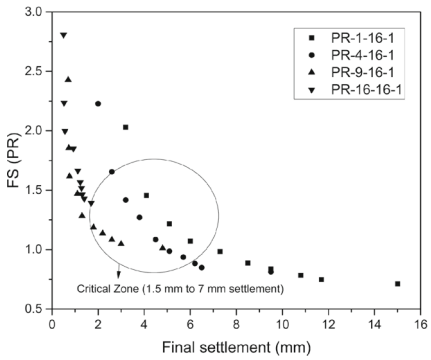

(b)

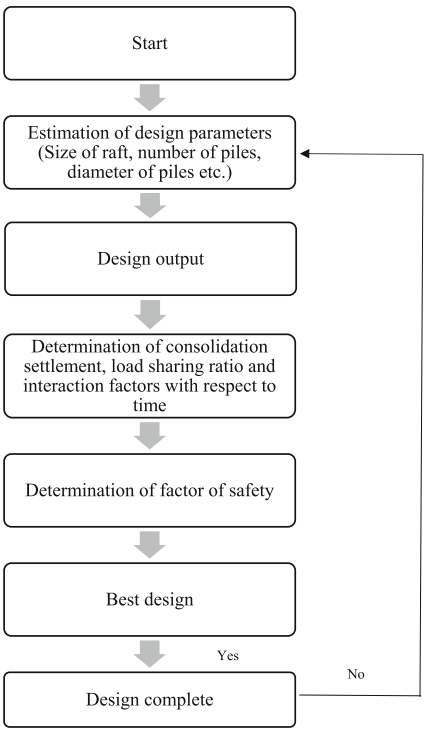

(c)

Fig. 14 **a** Factor of safety of PRF (PR-9-16-1) against the final (consolidation) settlement (for all the increments of load applied till the ultimate load for their respective time periods considered in the analysis) for both the numerical and predicted models, **b** factor of safety of PRFs having 1 m pile diameter and 16 m × 16 m raft, **c** design method of PRF

load applied till the ultimate load for their respective time periods considered in the analysis) for both the numerical and predicted models is plotted. From Fig. 14a, it is depicted that the results of the numerical model are quite similar with the predicted model having an error of 2.06–4.95%. This clarifies the accuracy of the proposed equations and the numerical model, which ensures the safe design of PRF.

The FS for different PRF configurations has been evaluated. A critical zone for FS has been obtained. Figure 14b shows the factor of safety of PRFs having 1 m pile diameter and 16 m × 16 m raft. A critical zone has been observed where the settlement lies between 1.5 and 7 mm. It is depicted that FS decreases with the increase in final settlement. The reduction rate of FS is high in low settlement magnitude. The reduction rate of FS is insignificant and nearly minimizes to a constant value at higher settlement magnitude. A critical zone has been suggested based on the non-uniform reduction rate of FS. It is depicted that the decrease in FS of PRF becomes insignificant when the settlement approaches 7 mm.

The load sharing ratio and the interactions factors have been determined by using the predicted equations and are authenticated with the numerical analysis results. A method for the estimation of FS of PRF has been developed. The design method of PRF developed is shown in the flowchart given in Fig. 14c.

6.5 Variation of Average, Differential and Reference Settlements with Time

The settlement has been obtained at three positions:

i. The centre point of raft
ii. The corner point of raft
iii. Point at a distance of 1/4th from the corner

The differential settlement (Δ_{c-c}), average settlement (Δ_{avg}) and the reference settlement (Δ_{ref}) are found out by the following equations [43]:

$$\Delta_{c-c} = \Delta_{\text{centre}} - \Delta_{\text{corner}} \tag{28}$$

$$\Delta_{\text{avg}} = (2\Delta_{\text{centre}} + \Delta_{\text{corner}})/3 \tag{29}$$

$$\Delta_{\text{ref}} = (\Delta_{\text{centre}} + 2\Delta_{1/4} + 2\Delta_{\text{corner}})/5 \tag{30}$$

where, Δ_{centre} denotes settlement at centre point of raft; Δ_{corner} denotes settlement at corner point of raft; and $\Delta_{1/4}$ denotes settlement at a point at a distance of 1/4th from the corner.

The differential and reference settlements are the important factors for increase in the internal stress inside the superstructure. It creates a negative influence by minimizing

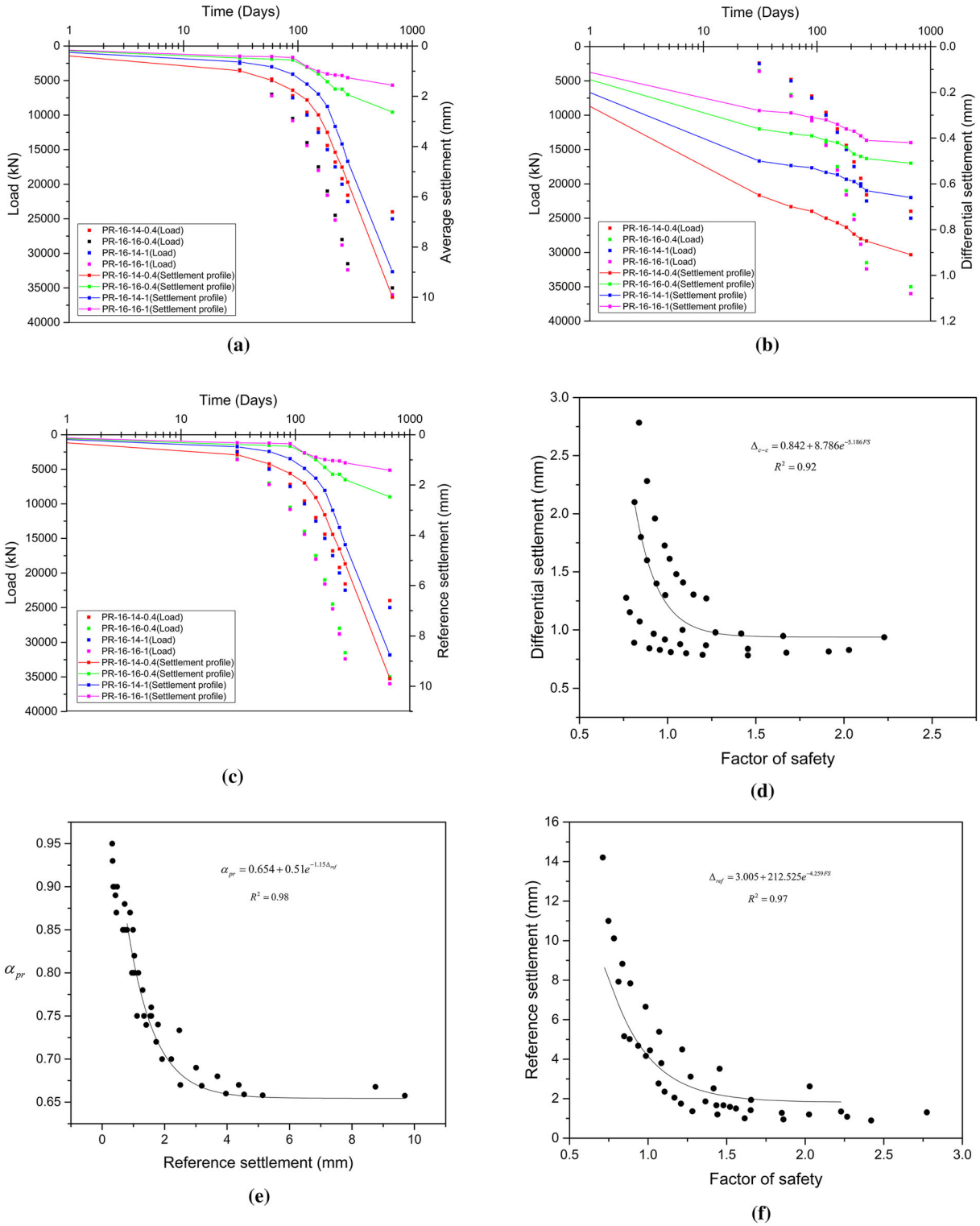

Fig. 15 **a** Average settlements with respect to time for each increment of loading for different raft widths and pile diameter consisting of 16 number of piles (4 × 4 pile group) in the PRFs, **b** Differential settlements with respect to time for each increment of loading for different raft widths and pile diameter consisting of 16 number of piles (4 × 4 pile group) in the PRFs, **c** Reference settlements with respect to time for each increment of loading for different raft widths and pile diameter consisting of 16 number of piles (4 × 4 pile group) in the PRFs, **d** Differential settlement for each increment of loading against the FS for PRFs consisting of raft width 16 m and pile diameter 1 m, **e** Load sharing ratio (α_{pr}) against the reference settlement for each increment of loading in the PRF consisting of different raft widths and pile diameter for 16 number of piles, **f** Reference settlement for each increment of loading against the FS for PRFs consisting of raft width 16 m and pile diameter 1 m

the service period of the superstructure below which PRF has been provided. A minimum amount of differential settlement can be attained by placing the PG in the central part of a flexible raft. The average, differential and reference settlements with respect to time for each increment of loading for different raft widths and pile diameter consisting of 16 number of piles (4 × 4 pile group) in the PRFs are obtained. The average settlements with respect to time for each increment of loading for different raft widths and pile diameter consisting of 16 number of piles (4 × 4 pile group) in the PRFs are presented in Fig. 15a. The differential settlements with respect to time for each increment of loading for different raft widths and pile diameter consisting of 16 number of piles (4 × 4 pile group) in the PRFs are presented in Fig. 15b. The reference settlements with respect to time for each increment of loading for different raft widths and pile diameter consisting of 16 number of piles (4 × 4 pile group) in the PRFs are presented in Fig. 15c. It can be depicted that the average, differential and reference settlements of PR-16-14-0.4 at the end of 22 months are 12–55%, 30–38% and 11–67% more than the average, differential and reference settlements of PR-16-14-1, respectively. Also, the average, differential and reference settlements of PR-16-16-0.4 at the end of 22 months are 20–69%, 21–29% and 21–75% more than the average, differential and reference settlements of PR-16-16-1, respectively. The average, differential and reference settlements with respect to time curves for each increment of loading show extremely nonlinear pattern. The PRF having larger number of piles, larger diameter of piles and larger raft width contribute to lesser average, differential and reference settlements than smaller number of piles, smaller diameter of piles and smaller raft width. It may be due to the increase in stiffness and surface area of PRF as the number of piles, diameter of piles and width of raft increases which leads to lesser settlement.

Figure 15d shows the differential settlement for each increment of loading against the FS for PRFs consisting of raft width 16 m and pile diameter 1 m. An exponential relationship is established showing a goodness of fit with $R^2 = 0.92$. It implies that the differential settlement has a significant impact for ensuring the safety level for superstructures. Δ_{c-c} is slowly decreased with the increase in FS of the PRF. An exponential relation is obtained from the best fitted curve as:

$$\Delta_{c-c} = 0.842 + 8.786e^{-5.186FS} \tag{31}$$

Figure 15e shows the load sharing ratio (α_{pr}) against the reference settlement for each increment of loading in the PRF consisting of different raft widths and pile diameter for 16 number of piles. An exponential relationship is established showing a goodness of fit with $R^2 = 0.98$. The relationship between α_{pr} and the reference settlement can be given as:

$$\alpha_{pr} = 0.654 + 0.51e^{-1.15\Delta_{\text{ref}}} \tag{32}$$

It implies that α_{pr} has a significant effect on the reference settlement of PRF. An increase in the α_{pr} indicates an increase in the foundation stiffness, which leads to decrease in the reference settlement. The reference settlement increases from 49 to 54% as the value of α_{pr} decreases for all the configurations of PRFs considered. The nonlinear behaviour of α_{pr} with the reference settlement can be executed for the optimized design of PRF.

Figure 15f shows the reference settlement for each increment of loading against the FS for PRFs consisting of raft width 16 m and pile diameter 1 m. An exponential expression has been established showing a goodness of fit with $R^2 = 0.97$. The relationship between the reference settlement and FS can be given as:

$$\Delta_{\text{ref}} = 3.005 + 212.525e^{-4.259FS} \tag{33}$$

The reference settlement decreases in a nonlinear manner with the FS. It is depicted from Fig. 15f that the reference settlement of PRFs consisting of raft width 16 m and pile diameter 1 m decreases from 14 to 1.5 mm as the FS increases from 0.75 to 2.80. A similar trend has been observed for all the PRF configurations. The expression ensures the influence of reference settlement on the FS and hence on the serviceability of any structure. Δ_{ref} refers to the minimal average displacement in the PRF as it considers the settlement of PRF at its centre and corner point of raft, and point at a distance of 1/4th from the corner. The determination of FS with respect to Δ_{ref} is necessary as it can create a negative influence by minimizing the service period of PRF as discussed above.

6.6 Variation of Water Table with the Final Settlement

The previous analyses have been carried out for the water table located at 7.5 m depth. The variation in water table affects the load-carrying capacity of the PRFs as well as the consolidation settlement of soil. The water table has been taken at the ground surface, 7.5 m and 10 m depths below ground surface. A dry condition (i.e. no water table) case has also been considered. The load-carrying capacity of PRFs for dry condition is the maximum, and the load-carrying capacity of PRFs for water table located at top surface is the minimum. For comparison of settlements, the PR-4-14-0.4 has been subjected to a vertical load of 11,000 kN which is being applied in increments of 10%. For each increment of loading, the settlement has been observed for a period of 1 month, and for the last increment, the settlement has been observed for a period of 1 year. Consolidation analysis has been carried out for each step. The settlement–time curves for the PRF

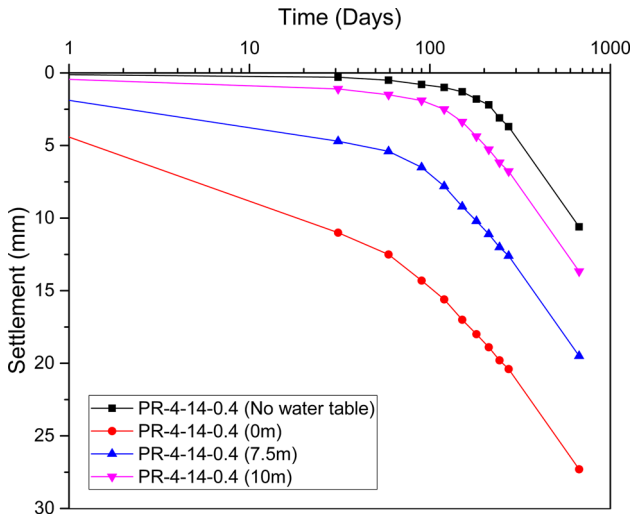

Fig. 16 Settlement–time curves for the PRF (PR-4-14-0.4) at different water table levels and dry condition

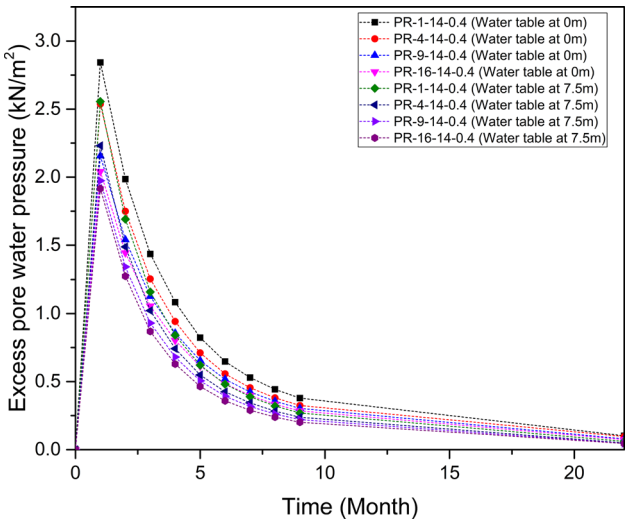

Fig. 17 Excess pore water pressure variations in soil having water table at 0 m and 7.5 m of PRFs having width of raft as 14 m and diameter of pile as 0.4 m with time

(PR-4-14-0.4) at different water table levels and dry condition are shown in Fig. 16. It can be depicted from Fig. 16 that the settlement of PR-4-14-0.4 at the end of 22 months corresponding to water table located at ground surface (0 m) is 157.54% more than the settlement corresponding to dry condition case (no water table). However, the settlements of PR-4-14-0.4 at the end of 22 months corresponding to water table located at 7.5 m and 10 m are 40% and 99.7% less than the settlement corresponding to water table located at ground surface (0 m), respectively. The settlements of PR-4-14-0.4 at the end of 22 months corresponding to water table located at 7.5 m and 10 m are 83.96% and 29.24% more than the settlement corresponding to dry condition (no water table) case, respectively. Hence, it can be concluded that very large amount of variation in settlement of PR-4-14-0.4 has been observed between the settlements corresponding to dry condition case, water tables located at 7.5 m and 10 m case. A remarkable amount of variation in settlement of PR-4-14-0.4 has been observed when the water table is located at ground surface and dry condition case. Similar trends have been observed for other PRF configurations considered. The curves show maximum settlement for water table located at the ground surface (0 m) and minimum settlement for dry condition case. The portion just below the raft experience maximum settlement. The settlement decreases as the depth increases.

6.7 Excess Pore Water Pressure (PWP) Variations with Respect to Time

The excess pore water pressure variations in soil with respect to a time period of 22 months at a depth of 8 m below the raft centre are evaluated for all the PRFs subjected to a vertical load of 11,000 kN which is being applied in increments of 10%. The settlement has been observed for a period of 1 month for each increment of loading, and the settlement has been observed for a period of 1 year for the last increment. Consolidation analysis has been carried out for each step. Figure 17 illustrates a typical plot for the excess pore water pressure variations in soil having water table at 0 m and 7.5 m of PRFs having width of raft as 14 m and diameter of pile as 0.4 m with time. The excess PWP is higher for a smaller number of piles because the soil is less confined compared to larger number of piles. The excess PWP in the soil remains maximum till 30 days after the application of load. Afterwards, it is rapidly decreased with time. The excess PWP is 30–33.33% higher for PRF consisting of single pile compared to PRF consisting of 4 × 4 pile group at the end of 22 months. The excess PWP in soil for PRFs having water table at 0 m has greater value than water table at 7.5 m. The excess PWP in soil for PRFs having water table at 0 m at the end of 22 months is about 40–42.85% greater than PRFs having water table at 7.5 m, respectively.

7 Multiple Linear Regression Analysis for Prediction of consolidation Settlement of PRF Under Vertical Loading

The proposed equations mentioned in the previous sections to estimate the consolidation settlement and ultimate load capacity of PRFs depend on several parameters like number and diameter of piles, width of raft and location of water table. To predict the consolidation settlement with respect

to time in low plasticity clay and intermediate plasticity clay (Kanpur soil) corresponding to the ULC of the PRFs, a generalized equation has been proposed incorporating the important parameters like number of piles (n), diameter of piles (d), width of raft (B_r), water table variation (W.T), ultimate load capacity ($Q_{pr,ult}$) and time (t). Multiple linear regression analysis has been performed to predict the consolidation settlement considering these influential parameters.

Multiple linear regression method is a regression analysis for predicting the correlation between a dependent variable with more than one independent variables. The fact is clear that consolidation settlement of soil depends on the amount of load applied on the PRF, time taken and all the parameters mentioned earlier. Hence, consolidation settlement (x) can be expressed as a function of six independent variables, i.e. n, d, B_r, W.T, $Q_{pr,ult}$ and t. x can be expressed as:

$$x = f(n,\ d,\ B_r,\ \text{W.T},\ Q_{pr,ult},\ t) \tag{34}$$

Equation (34) can be written in the form of linear regression including intercept and coefficients as:

$$x = c_0 + c_1 n + c_2 d + c_3 B_r + c_4 W.T + c_5 Q_{pr,ult} + c_6 t \tag{35}$$

where c_0 denotes the intercept and c_1, c_2, c_3, c_4, c_5 and c_6 denote coefficients of the independent variables n, d, B_r, W.T, $Q_{pr,ult}$ and t, respectively. The intercept and coefficients have been calculated using ANOVA statistical model based on multiple linear regression analysis. The independent variables are assumed linear in ANOVA, and least square estimation has been used to estimate the consolidation settlement. A total number of 96 observations have been considered for the analysis for low plasticity clay and intermediate plasticity clay (Kanpur soil). The set of 96 observations of dependent (x) and independent (n, d, B_r, W.T, $Q_{pr,ult}$ and t) variables are presented in Table 10. 't' has been taken as 10 months and 22 months in Table 10 as for the following PRFs mentioned, $Q_{pr,ult}$ has been applied at 10 months and the settlement has been observed for 12 months (1 year) after the loading has been applied as mentioned in the method of analysis section. For the initial 9 months, stage-wise increment of 10% of $Q_{pr,ult}$ has been provided. For each increment of loading, the settlement has been observed for 1 month as mentioned earlier. Table 11 presents the values of intercept, coefficients and statistical regression parameters calculated using ANOVA. The values of the intercept and coefficients as mentioned in Eq. (35) are summarized in Table 11. Also, the statistical regression parameters such as Multiple R, R square, Adjusted R square, F value and Significance F are presented. Generally, Multiple R (correlation coefficient) value lies between + 1 and − 1. Multiple R depicts the tandem movement of the dependent and independent variables. Multiple R value of + 1 depicts that the variables proceed ideally in tandem together in the same direction. Table 11 shows that Multiple R value is very close to + 1 which indicates that the variables are mostly in tandem with each other. R square value is 0.935 which is very close to 1. It indicates a very good fit between the parameters and regression line. Additionally, the 'Significance F' value calculated from the 'F value' is remarkably very small which indicates negligible probability of the inaccuracy of the regression model. Therefore, the intercept and coefficient values acquired by ANOVA using Eqs. (34) and (35) are reliable and can be implemented for the rational design of PRFs subjected to vertical loading in low plasticity clay and intermediate plasticity clay with clay percentage varying between 6 and 22%. Thus, the consolidation settlement (x) can be expressed as:

$$x = 55.61 - 0.305n - 1.138d - 1.735B_r - 1.146W.T - 0.00035Q_{pr,ult} + 0.287t \tag{36}$$

where the units of d, B_r and W.T are taken in 'm'. The units for $Q_{pr,ult}$ and t are taken in 'kN' and 'month', respectively.

8 Validation of the Proposed Design Equation Using an Example

The motive of this section is to estimate the ultimate load capacities and consolidation settlements of PRFs by using PLAXIS 3D as well as proposed equation mentioned in the previous section. For the design purpose, a raft size of 10 m × 10 m × 1 m has been considered to be placed on Kanpur soil (Table 1). The water table has been considered at 7.5 m. 25 number of piles of length and diameter of 20 m and 0.6 m, respectively, are considered to be embedded symmetrically in the soil. The piles are rigidly connected to the raft. The spacing between the piles is taken as 3d. The Young's modulus and unit weight of raft and piles are taken as 29×10^6 kN/m^2 and 24 kN/m^3, respectively. The ultimate load capacity of the PRF obtained from PLAXIS 3D is 52,000 kN. The vertical loading has been applied in increments of 10% of the ultimate load capacity. For each increment of loading, the settlement has been observed for a time period of 1 month, and for the ultimate load, the settlement has been observed for a period of 5 years. The vertical settlement contour of the PRF consisting of 5 × 5 pile group with spacing between the piles as 3d is shown in Fig. 18a. The final vertical settlement has been obtained as 22.58 mm as depicted in Fig. 18a. However, if the spacing between the piles is considered as 4d, then the final settlement has been obtained as 20.34 mm. The vertical settlement contour of the PRF consisting of 5 × 5 pile group with spacing between the piles

Table 10 Set of 96 observations of dependent (x) and independent (n, d, B_r, $W.T$, $Q_{pr,ult}$ and t) variables

	Dependent variable	Independent variables					
	x (mm)	n	d (m)	B_r (m)	$W.T$ (m)	$Q_{pr,ult}$(kN)	t(month)
PR-1-14-0.4	24.5	1	0.4	14	7.5	24,000	22
	17.3	1	0.4	14	7.5	24,000	10
	32.8	1	0.4	14	0	23,300	22
	26.3	1	0.4	14	0	23,300	10
	19.08	1	0.4	14	10	24,300	22
	12.77	1	0.4	14	10	24,300	10
PR-4-14-0.4	19.5	4	0.4	14	7.5	29,000	22
	13.2	4	0.4	14	7.5	29,000	10
	27.3	4	0.4	14	0	28,100	22
	20.9	4	0.4	14	0	28,100	10
	13.67	4	0.4	14	10	29,100	22
	7.1	4	0.4	14	10	29,100	10
PR-9-14-0.4	13.8	9	0.4	14	7.5	38,000	22
	9.1	9	0.4	14	7.5	38,000	10
	21.4	9	0.4	14	0	37,400	22
	16.3	9	0.4	14	0	37,400	10
	7.97	9	0.4	14	10	38,200	22
	3	9	0.4	14	10	38,200	10
PR-16-14-0.4	10.3	16	0.4	14	7.5	41,000	22
	6.4	16	0.4	14	7.5	41,000	10
	17.9	16	0.4	14	0	40,500	22
	13.6	16	0.4	14	0	40,500	10
	4.47	16	0.4	14	10	41,300	22
	0.3	16	0.4	14	10	41,300	10
PR-1-16-1	15	1	1	16	7.5	30,000	22
	12.4	1	1	16	7.5	30,000	10
	22.8	1	1	16	0	29,400	22
	19.3	1	1	16	0	29,400	10
	9.26	1	1	16	10	30,400	22
	6.45	1	1	16	10	30,400	10
PR-4-16-1	9.5	4	1	16	7.5	35,000	22
	7.1	4	1	16	7.5	35,000	10
	17.1	4	1	16	0	34,300	22
	14.2	4	1	16	0	34,300	10
	4.06	4	1	16	10	35,500	22
	1.25	4	1	16	10	35,500	10
PR-9-16-1	4.8	9	1	16	7.5	48,000	22
	3.4	9	1	16	7.5	48,000	10
	12.2	9	1	16	0	47,600	22
	9.9	9	1	16	0	47,600	10
	1.46	9	1	16	10	48,400	22
	1.24	9	1	16	10	48,400	10
PR-16-16-1	1.7	16	1	16	7.5	51,000	22

Table 10 (continued)

	Dependent variable			Independent variables			
	x (mm)	n	d (m)	B_r (m)	$W.T$ (m)	$Q_{pr,ult}$(kN)	t(month)
	1.45	16	1	16	7.5	51,000	10
	8.7	16	1	16	0	50,400	22
	5.8	16	1	16	0	50,400	10
	1.23	16	1	16	10	51,200	22
	1.02	16	1	16	10	51,200	10
PR-1-16-0.4	17	1	0.4	16	7.5	28,000	22
	14.1	1	0.4	16	7.5	28,000	10
	24.98	1	0.4	16	0	27,600	22
	22.12	1	0.4	16	0	27,600	10
	11.34	1	0.4	16	10	28,300	22
	8.65	1	0.4	16	10	28,300	10
PR-4-16-0.4	12	4	0.4	16	7.5	32,000	22
	9.1	4	0.4	16	7.5	32,000	10
	19.8	4	0.4	16	0	31,600	22
	17.7	4	0.4	16	0	31,600	10
	6.26	4	0.4	16	10	32,600	22
	3.45	4	0.4	16	10	32,600	10
PR-9-16-0.4	6.3	9	0.4	16	7.5	43,000	22
	4.1	9	0.4	16	7.5	43,000	10
	14.1	9	0.4	16	0	42,500	22
	12.1	9	0.4	16	0	42,500	10
	1.56	9	0.4	16	10	43,400	22
	1.35	9	0.4	16	10	43,400	10
PR-16-16-0.4	2.8	16	0.4	16	7.5	50,000	22
	2.2	16	0.4	16	7.5	50,000	10
	9.8	16	0.4	16	0	49,700	22
	8.3	16	0.4	16	0	49,700	10
	1.34	16	0.4	16	10	50,200	22
	1.12	16	0.4	16	10	50,200	10
PR-1-14-1	22.5	1	1	14	7.5	26,000	22
	15	1	1	14	7.5	26,000	10
	30.3	1	1	14	0	25,700	22
	24.8	1	1	14	0	25,700	10
	17.5	1	1	14	10	26,400	22
	10.47	1	1	14	10	26,400	10
PR-4-14-1	17	4	1	14	7.5	30,000	22
	12.8	4	1	14	7.5	30,000	10
	24.34	4	1	14	0	29,500	22
	19.67	4	1	14	0	29,500	10
	10.96	4	1	14	10	30,400	22
	6.56	4	1	14	10	30,400	10
PR-9-14-1	12.3	9	1	14	7.5	39,000	22

Table 10 (continued)

	Dependent variable			Independent variables			
	x (mm)	n	d (m)	B_r (m)	$W.T$ (m)	$Q_{pr,ult}$(kN)	t(month)
	7.8	9	1	14	7.5	39,000	10
	20.4	9	1	14	0	38,600	22
	18.3	9	1	14	0	38,600	10
	7.23	9	1	14	10	39,500	22
	4.54	9	1	14	10	39,500	10
PR-16-14-1	9.2	16	1	14	7.5	42,000	22
	5.6	16	1	14	7.5	42,000	10
	16.5	16	1	14	0	41,300	22
	13.4	16	1	14	0	41,300	10
	3.75	16	1	14	10	42,400	22
	1.23	16	1	14	10	42,400	10

as 4d is shown in Fig. 18b. It is implied that increase in the spacing of piles in PRF leads to lesser settlement. For smaller spacing of piles, the developed stress field around the piles overlap each other due to vertical load. However, in case of larger spacing, the overlapping of stress fields is negligible, resulting in a lesser interaction effect of piles. For the validation with the proposed equation for the first case, considering the ultimate load as 52,000 kN and putting all the values in Eq. (36), a final settlement of 23.25 mm has been obtained which is 2.96% more than the settlement obtained through the numerical analysis. For the second case, 53,000 kN has been obtained as the ultimate load capacity. By putting all the values in Eq. (36) for the second case, a final settlement of 22.9 mm has been obtained which is 12.58% more than the settlement obtained through the numerical analysis. The design example depicts that for spacing of piles taken as 4d in the PRF, the consolidation settlement is about 11% lesser as obtained by numerical analysis and 1.52% lesser as obtained by the predicted equation than when the spacing of piles is taken as 3d in the PRF. Hence, the predicted equation shows reliable settlement with an error of 2.96–12.58% for low and intermediate plasticity clay with clay percentage varying between 6 and 22% and therefore can be used for the estimation of consolidation settlement of PRFs subjected to incremental compressive loading.

Table 11 Values of intercept, coefficients and statistical regression parameters calculated using ANOVA

Type of soil	Regression parameters, intercept and coefficients	Design equation x
Low and intermediate plasticity clay with clay percentage varying between 6 and 22%	Multiple R	0.967453
	R Square	0.935966
	Adjusted R square	0.931649
	F value	216.8136
	Significance F	7.14E−51
	c_0	55.61377
	c_1	− 0.30542
	c_2	− 1.13897
	c_3	− 1.73508
	c_4	− 1.14604
	c_5	− 0.00035
	c_6	0.287361

9 Recommendations for Future Studies

Some recommendations for future studies related to the topic are to develop performance-based design criteria for piled-raft foundations to ensure acceptable levels of performance under various loading scenarios such as vertical, lateral and moment loading. This could involve establishing performance metrics, such as acceptable levels of settlement or differential settlement, and designing foundations that meet these criteria while considering factors such as soil variability and future changes in loading conditions. The future studies can also involve to investigate the environmental impact of piled-raft foundations and explore sustainable design approaches. This may involve assessing the carbon footprint associated with construction materials, exploring alternative eco-friendly materials and evaluating the long-term effects of pile–raft foundations on the surrounding environment. The development of Load and Resistance Factor Design (LRFD) methods specifically tailored for pile–raft foundations can be explored in the future studies. This would involve incorporating reliability-based approaches to determine design loads

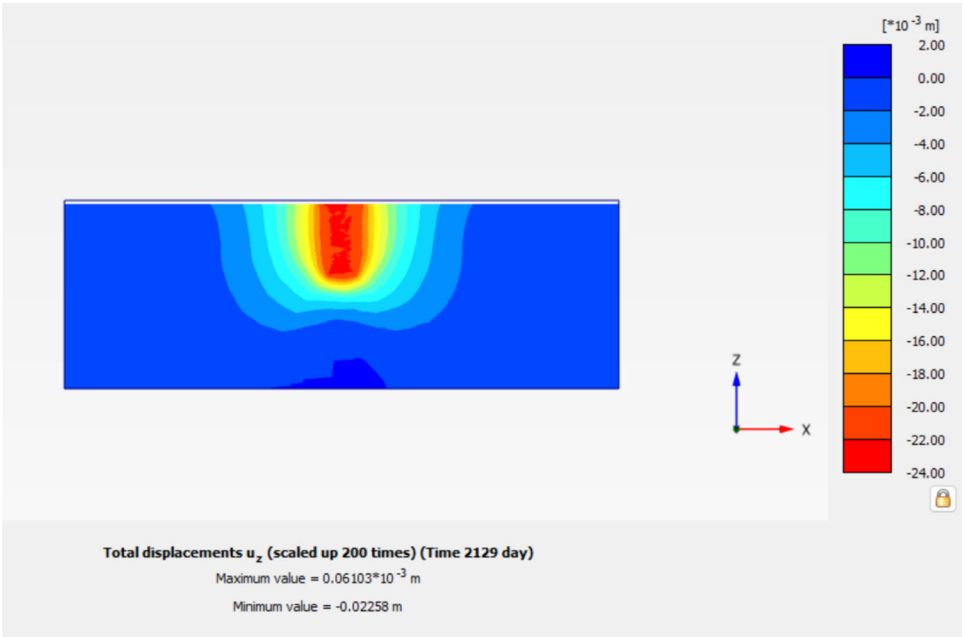

(a)

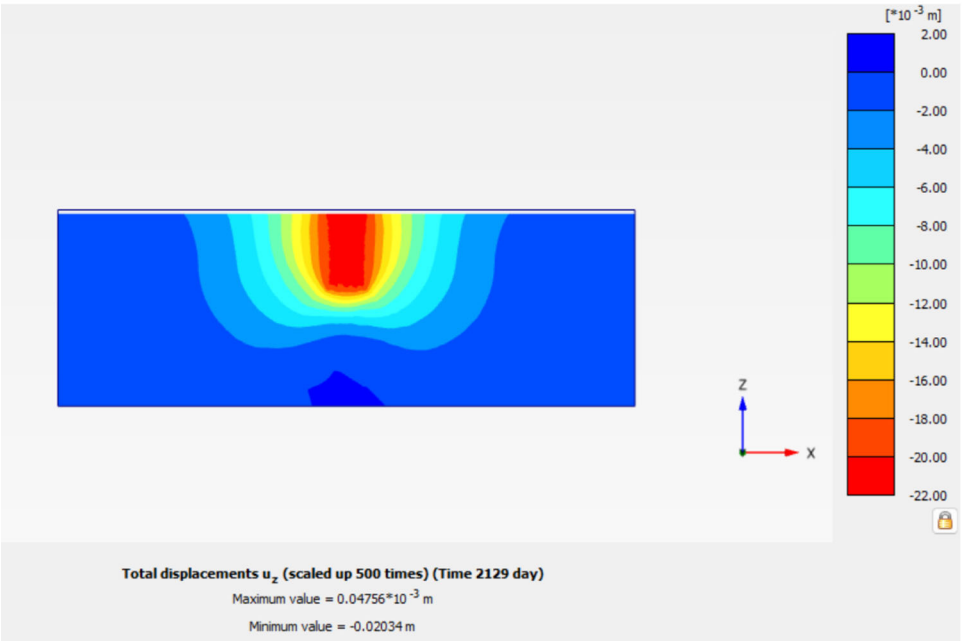

(b)

Fig. 18 **a** Vertical settlement contour of the PRF consisting of 5×5 pile group with spacing between the piles as $3d$, **b** Vertical settlement contour of the PRF consisting of 5×5 pile group with spacing between the piles as $4d$

and resistance factors considering the uncertainties associated with soil properties, loads and structural response.

10 Conclusions

The following conclusions can be justified from the context:

- The final (consolidation) settlement obtained after a time period of 22 months is about 15–30% higher than the settlement obtained using plastic analysis corresponding to the ULC of the PRFs.
- The long-term (consolidation) settlement shows noticeable nonlinearity as pronounced from the settlement–time plots. The final settlement including the immediate and consolidation settlements obtained at the end of 22 months is about 240–1050% more than the immediate settlement

obtained at the end of 1 month for all the foundation systems considered.

- As the number of piles, pile diameter and width of raft increases, α_{pr} increases by about 34–48%, 6–19% and 11–20%, respectively, as a greater number of piles and a larger pile diameter will help to support more load. If the raft width increases, then the soil confinement also increases which increases the pile mobilization, hence enhancing the load capacity of PRF. As the time increases for each load increment, the final settlement increases, while the α_{pr} value decreases for all the PRFs considered.
- The interaction effects of the PRF have been considered for each configuration, and the interaction factors have been calculated. Suitable evaluation of interaction factors and load sharing ratio considering consolidation settlement of soil in PRFs has been proposed. The numerical analysis has been utilized to model an interrelationship among the interaction factors, LSR and LDC.
- β_{pr} initially increases up to a final settlement of 9 mm and then gradually decreases due to the further settlement of raft. The highest value of β_{pr} obtained is 1.2. It has been observed that the pile–raft interaction factor (β_{pr}) increases with the increasing magnitude of final settlement. β_{pr} becomes more than unity at higher magnitude of final (consolidation) settlement. The lower value of β_{pr} indicates early mobilization of shaft (skin) friction of pile generating lesser contact pressure between soil and raft.
- β_{rp} value decreases up to a final settlement of 5 mm and increases thereafter. It is due to the further settlement of raft because of the incremental vertical loading. The lowest and highest values of β_{rp} are 0.5 and 1.8 corresponding to the final settlement level of 15.3 mm and 0.5 mm, respectively. β_{rp} decreases initially because of the fast mobilization of load capacity of piles at the initial increments of loading which leads to a lesser pressure surrounding the contact area between the soil and the raft near the piles. β_{rp} increases afterwards because of the raft starting to take load as the final settlement increases.
- The determination of FS with respect to Δ_{ref} is necessary as it can create a negative impact by minimizing the service period of the PRF. Δ_{ref} decreases in a nonlinear manner with the FS.
- All the suggested prediction models have been used to get the overall FS of PRFs, and design of PRF has been suggested keeping in view the safety and serviceability.
- The excess PWP is higher for a smaller number of piles because the soil is less confined compared to larger number of piles. The excess PWP in the soil remains maximum till 30 days after the application of load. Afterwards, it is rapidly decreased with time.
- The proposed equation developed by the multiple regression analysis has been validated using a design example and is reliable to predict consolidation settlement of PRFs considering time effect particularly for low plasticity clay and intermediate plasticity clay with clay percentage varying between 6 and 22%.

Acknowledgements The authors express their gratitude for the financial support provided by Board of Research in Nuclear Sciences (BRNS) (Grant No. 2018-BRNS/10195).

Author Contributions KT contributed to conceptualization, data curation, formal analysis, investigation, validation and writing—original draft. NRP was involved in methodology, project administration, supervision, visualization and writing—review and editing. SR contributed to supervision and writing—review and editing. AM was involved in funding acquisition, project administration and writing—review and editing.

Funding The work has been supported by Board of Research in Nuclear Sciences (BRNS) (Grant No. 2018-BRNS/10195).

Data Availability Authors can confirm that all relevant data are included in the article and/or its supplementary information files.

Code Availability PLAXIS 3D.

Declarations

Conflict of interest On behalf of all authors, the corresponding author states that there is no conflict of interest.

References

1. Poulos, H.G.: Piled raft foundations: design and applications. Geotechnique **51**(2), 95–113 (2001)
2. El-Mossallamy, Y.: Innovative application of piled raft foundation in stiff and soft subsoil. In: Deep Foundations 2002: an international perspective on theory, design, construction, and performance, 426–440 (2002)
3. Burland, J.B.; Broms, B.B.; De Mello, V.F.B.: Behaviour of foundation and structures. In: Proceedings of the 7th international conference on SMFE, Tokyo, 1: 495–546 (1977)
4. Bowles, J.E.: Foundation analysis and design (1988)
5. Katzenbach, R.; Arslan, U.; Moormann, C.: Chapter 13 Piled raft foundation projects in Germany. In: Hemsley, J.A. (Ed.) Design applications of raft foundations, pp. 323–391. Thomas Telford, London (2000)
6. Yamashita, K.; Hamada, J.; Onimaru, S.; Higashino, M.: Seismic behavior of piled raft with ground improvement supporting a base-isolated building on soft ground in Tokyo. Soils Found. **52**(5), 1000–1015 (2012)
7. Lee, J.; Park, D.; Park, D.; Park, K.: Estimation of load-sharing ratios for piled rafts in sands that includes interaction effects. Comput. Geotech. **63**, 306–314 (2015)
8. Cho, J.; Lee, J.H.; Jeong, S.; Lee, J.: The settlement behavior of piled raft in clay soils. Ocean Eng. **53**, 153–163 (2012)
9. Chung Nguyen, D.D.; Kim, D.S.; Jo, S.B.: Settlement of piled rafts with different pile arrangement schemes via centrifuge tests. J. Geotech. Geoenviron. Eng. **139**(10), 1690–1698 (2013)
10. Deb, P.; Pal, S.K.: Analysis of load sharing response and prediction of interaction behaviour in piled raft foundation. Arab. J. Sci. Eng. **44**(10), 8527–8543 (2019). https://doi.org/10.1007/s13369-019-03936-1

11. Halder, P.; Manna, B.: A New model for the prediction of load sharing in piled raft system—an experimental investigation. Arab. J. Sci. Eng. **46**(11), 10667–10680 (2021)
12. Mali, S.; Singh, B.: Behavior of large piled-raft foundation on clay soil. Ocean Eng. **149**, 205–216 (2018)
13. Hoang, L.T.; Matsumoto, T.: Long-term behavior of piled raft foundation models supported by jacked-in piles on saturated clay. Soils Found. **60**(1), 198–217 (2020)
14. Mattsson, N.; Menoret, A.; Simon, C.; Ray, M.: Case study of a full-scale load test of a piled raft with an interposed layer for a nuclear storage facility. Géotechnique **63**(11), 965–976 (2013)
15. Rodriguez Rincon, E.; Cunha, R.P.D.; Caicedo Hormaza, B.: Analysis of settlements in piled raft systems founded in soft soil under consolidation process. Can. Geotech. J. **57**(4), 537–548 (2020)
16. Roy, S.; Chattopadhyay, B.C.; Sahu, R.B.: Piled-raft foundation behavior on consolidating soft soil. In: Proceedings of the Indian geotechnical conference, Kochi, India, 879–882 (2011)
17. Tarenia, K.; Patra, N.R.: Behaviour of disconnected and connected piled-raft foundations subjected to vertical and lateral loads simultaneously. In: Geo congress 2020: foundations, soil improvement, and erosion. Reston, VA: American Society of Civil Engineers, 33–44 (2020)
18. Tarenia, K.; Patra, N.R.: Long-term effect of vertical and lateral loads on piled raft foundations: a case study. Proc. Inst. Civ. Eng. Geotech. Eng. (2022). https://doi.org/10.1680/jgeen.22.00030
19. Tarenia, K.; Patra, N.R.; Sathiyamoorthy, R.; Mondal, A.: Behaviour of rigid piled- raft foundation subjected to compressive loading considering time effect: experimental and analytical study. Int. J. Geomech. (2023). https://doi.org/10.1061/IJGNAI.GMENG-8713
20. Thaher, M.; Jessberger, H.L.: The behavior of pile-raft foundations, investigated in centrifuge model tests. In: Centrifuge 91: proceedings of the international conference centrifuge, boulder, Colo. ISMFE, 225–23 (1991)
21. Yamashita, K.; Yamada, T.; Hamada, J.: Investigation of settlement and load sharing on piled rafts by monitoring full-scale structures. Soils Found. **51**(3), 513–532 (2011)
22. de Sanctis, L.; Mandolini, A.: Bearing capacity of piled rafts on soft clay soils. J. Geotech. Geoenviron. Eng. **132**(12), 1600–1610 (2006)
23. Horikoshi, K.; Randolph, M.F.: Centrifuge modelling of piled raft foundations on clay. Geotechnique **46**(4), 741–752 (1996)
24. Katzenbach, R.; Schmitt, A.; Turek, J.: Assessing settlement of high-rise structures by 3D simulations. Comput. Aided Civ. Infrastruct. Eng. **20**(3), 221–229 (2005)
25. Long, P.D.: Footings with settlement-reducing piles in non-cohesive soil. Ph.D. thesis, Chalmers University of Technology, Gothenburg, Sweden (1993)
26. Han, J.; Ye, S.L.: A field study on the behavior of a foundation underpinned by micropiles. Can. Geotech. J. **43**(1), 30–42 (2006)
27. Horikoshi, K.; Randolph, M.F.: A contribution to optimum design of piled rafts. Geotechnique **48**(3), 301–317 (1998)
28. Liu, J.L.; Yuan, Z.L.; Shang, K.P.: Cap-pile-soil interaction of bored pile groups. In: Proceedings of the 11th Eleventh international conference on soil mechanics and foundation engineering (ICSMFE), San Francisco, 3: 1433–1436 (1985)
29. Reul, O.; Randolph, M.F.: Piled rafts in overconsolidated clay: comparison of in situ measurements and numerical analyses. Geotechnique **53**(3), 301–315 (2003)
30. Conte, G.; Mandolini, A.; Randolph, M.: Centrifuge modelling to investigate the performance of piled rafts. In: Centrifuge modelling to investigate the performance of piled rafts, Millpress, 359–366 (2003)
31. Park, D.; Lee, J.: Comparative analysis of various interaction effects for piled rafts in sands using centrifuge tests. J. Geotech. Geoenviron. Eng. **141**(1), 04014082 (2015)
32. PLAXIS 3D CE V20. Computer software. PLAXIS BV, Delft, Netherlands
33. Kumar, A.; Choudhury, D.; Katzenbach, R.: Effect of earthquake on combined pile–raft foundation. Int. J. Geomech. **16**(5), 04016013 (2016)
34. Nguyen, D.D.C.; Kim, D.S.; Jo, S.B.: Parametric study for optimal design of large piled raft foundations on sand. Comput. Geotech. **55**, 14–26 (2014)
35. Von Soos, P.: Properties of Soil and Rock (in German), Grundbau Taschenbuch Part 4. Ernst & Sohn, Berlin (1990)
36. Janbu, N.: Soil compressibility as determined by odometer and triaxial tests. In: Proc. Europ. Conf. SMFE, 1: 19–25 (1963)
37. Brinkgreve, R.B.J.; Swolfs, W.M.; Engin, E.; Waterman, D.; Chesaru, A.; Bonnier, P.G.; Galavi, V.: PLAXIS 3D 2010. User manual, Plaxis bv (2010)
38. Obrzud, R.F.: On the use of the hardening soil small strain model in geotechnical practice. Numer. Geotech. Struct. **16**, 1–17 (2010)
39. Poulos, H.G.; Davis, E.H.: Pile Foundation Analysis and Design. Wiley, New York (1980)
40. IS: 2911 (Part 4): Code of practice for design and construction of pile foundations, (1985)
41. IS 2911 (Part 1/sec 2): Code of practice for design and construction of pile foundations: Part 1 concrete piles, section 2 Bored cast In-Situ piles, (1979)
42. Kumar, A.; Choudhury, D.: Development of new prediction model for capacity of combined pile-raft foundations. Comput. Geotech. **97**, 62–68 (2018)
43. Reul, O.; Randolph, M.F.: Design strategies for piled rafts subjected to nonuniform vertical loading. J. Geotech. Geoenviron. Eng. **130**(1), 1–13 (2004)